Functional and Structural Diversification of the Anguimorpha Lizard Venom System*

Bryan G. Fry,[a,b] Kelly Winter,[c] Janette A. Norman,[a] Kim Roelants,[a,d] Rob J. A. Nabuurs,[e,f] Matthias J. P. van Osch,[e] Wouter M. Teeuwisse,[e] Louise van der Weerd,[e,f] Judith E. Mcnaughtan,[g] Hang Fai Kwok,[h] Holger Scheib,[i] Laura Greisman,[c] Elazar Kochva,[j] Laurence J. Miller,[k] Fan Gao,[k] John Karas,[l] Denis Scanlon,[l] Feng Lin,[m] Sanjaya Kuruppu,[c] Chris Shaw,[h] Lily Wong,[c] and Wayne C. Hodgson[c]

Venom has only been recently discovered to be a basal trait of the Anguimorpha lizards. Consequently, very little is known about the timings of toxin recruitment events, venom protein molecular evolution, or even the relative physical diversifications of the venom system itself. A multidisciplinary approach was used to examine the evolution across the full taxonomical range of this ~130 million-year-old clade. Analysis of cDNA libraries revealed complex venom transcriptomes. Most notably, three new cardioactive peptide toxin types were discovered (celestoxin, cholecystokinin, and YY peptides). The latter two represent additional examples of convergent use of genes in toxic arsenals, both having previously been documented as components of frog skin defensive chemical secretions. Two other novel venom gland-overexpressed modified versions of other protein frameworks were also recovered from the libraries (epididymal secretory protein and ribonuclease). Lectin, hyaluronidase, and veficolin toxin types were sequenced for the first time from lizard venoms and shown to be homologous to the snake venom forms. In contrast, phylogenetic analyses demonstrated that the lizard natriuretic peptide toxins were recruited independently of the form in snake venoms. The *de novo* evolution of helokinestatin peptide toxin encoding domains within the lizard venom natriuretic gene was revealed to be exclusive to the helodermatid/anguid subclade. New isoforms were sequenced for cysteine-rich secretory protein, kallikrein, and phospholipase A_2 toxins. Venom gland morphological analysis revealed extensive evolutionary tinkering. Anguid glands are characterized by thin capsules and mixed glands, serous at the bottom of the lobule and mucous toward the apex. Twice, independently this arrangement was segregated into specialized serous protein-secreting glands with thick capsules with the mucous lobules now distinct (*Heloderma* and the *Lanthanotus*/*Varanus* clade). The results obtained highlight the importance of utilizing evolution-based search strategies for biodiscovery and emphasize the largely untapped drug design and development potential of lizard venoms. ***Molecular & Cellular Proteomics 9:2369–2390, 2010.***

Because of significant differences in anatomy of the venom delivery system and distant phylogenetic relatedness, it had been long assumed that the venom systems of snakes and helodermatid lizards were independently evolved (1–3). However, both lineages were recently revealed to be members of a clade (Toxicofera) that also included several lineages of other lizards recently shown to be venomous (4, 5). In contrast to the hypothesis of independent origins, this new perspective revealed that lizard and snake venom systems are homologous but highly differentiated descendants of an early evolved venom system in squamates. The basal condition was incipient glands on both the mandibular and maxillary regions with snakes favoring the maxillary venom glands and secondarily losing the mandibular venom glands. However, the anguimorph lizards (anguids, helodermatids, and varanids) did the reverse, resulting in the modern condition seen today.

The lizard venom delivery system is less sophisticated than the high pressure injection mechanism of the front fanged advanced snakes, and the vast majority of the species pose trivial direct medical risks to human (with the exception of helodermatids and large varanids such as *Varanus komodoensis*). However, the effects of envenomation from medi-

From the [a]Venomics Research Laboratory, Department of Biochemistry and Molecular Biology, Bio21 Molecular Science and Biotechnology Institute and [g]Department of Pathology, University of Melbourne, Melbourne, Victoria 3000, Australia, [c]Monash Venom Group, Department of Pharmacology, Monash University, Clayton, Victoria 3800, Australia, [d]Unit of Ecology and Systematics, Biology Department, Vrije Universiteit Brussel, Pleinlaan 2, B-1050 Brussels, Belgium, Departments of [e]Radiology and [f]Anatomy and Embryology, Leiden University Medical Center, 2300 Leiden, The Netherlands, [h]Molecular Therapeutics Research, School of Pharmacy, Queen's University, Belfast BT7 1NN, Northern Ireland, [i]SBC Lab AG, Seebüelstrasse 26, 8185 Winkel, Switzerland, [j]Department of Zoology, Tel Aviv University, Tel Aviv 69978, Israel, [k]Mayo Clinic, Scottsdale, Arizona 85259, [l]Bio21 Molecular Science and Biotechnology Institute, University of Melbourne, Parkville, Victoria 3010, Australia, and [m]Howard Florey Institute, University of Melbourne, Victoria 3010, Australia

Received, May 30, 2010, and in revised form, July 12, 2010

Published, MCP Papers in Press, July 14, 2010, DOI 10.1074/mcp.M110.001370

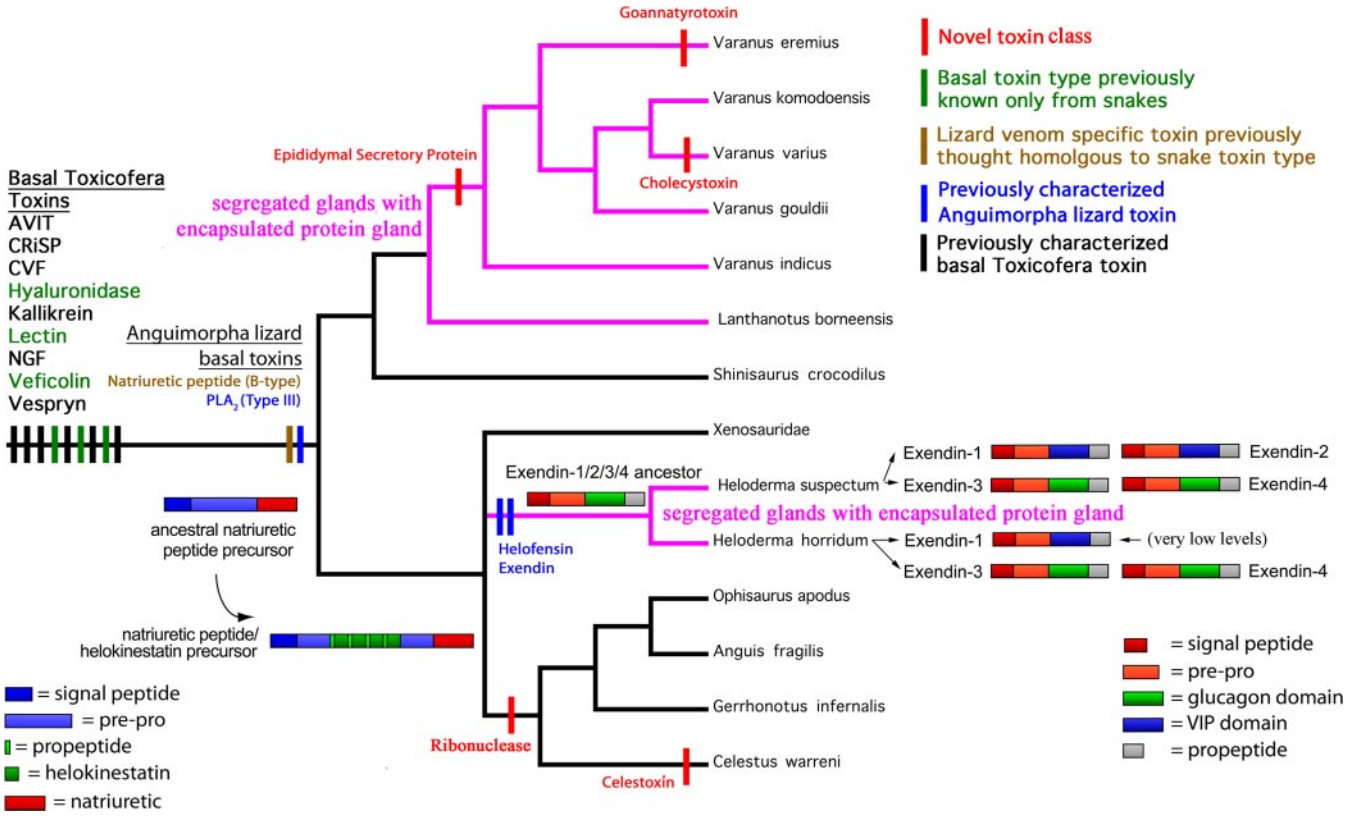

FIG. 1. **Cladogram of evolutionary relationships of representative Anguimorpha lizards (54) showing relative timing of toxin recruitment events and derivations of venom system.** *NGF*, nerve growth factor; *CVF*, cobra venom factor.

cally important species such as *Heloderma* (for example) may be clinically complex with symptoms, including extreme pain, acute local swelling, nausea, fever, faintness, myocardial infarction, tachycardia, hypotension, and inhibition of blood coagulation (6–12).

It has been shown previously that venoms evolve via toxin recruitment events. In this process, a gene encoding for a normal body protein (typically one involved in key regulatory processes or bioactivity) is duplicated, and the copy is selectively expressed in the venom gland (13). Toxins are sourced at different times during the evolutionary history from a wide range of tissues, are of disparate scaffolds, and have diverse ancestral bioactivities. Functionally important toxin types are reinforced through adaptive evolution involving explosive duplication and diversification, creating a venom gland-specific multigene family. The likelihood for neofunctionalization is increased through random mutation, gene conversion, and unequal crossing over (14). Although the molecular scaffold of the ancestral protein is conserved, derived activities emerge through mutations of the surface chemistry (14–17). Because of the inherent chemical arms race between venomous animals and their prey, toxins have exquisite biological targeting with sometimes as little as a single amino acid change radically changing specificity or potency.

Previous work demonstrated that a core set of venom genes evolved in the common Toxicofera ancestor (4), and subsequent toxin recruitment events facilitated diversification into complex and varied venoms (18–20) (Fig. 1). The anguimorph lizards, of which the helodermatid lizards were long thought to be the only venomous members, are a very large assemblage with great diversity in body size and ecological niche occupied (21). To date, only the venoms of two extant helodermatid lizards and a small, taxonomically limited handful of varanid lizard species have been studied with the anguid lizard clade almost entirely ignored. Currently, seven protein families have been identified as recruited for use as toxins in lizard venoms (see Table I): helofensin (lethal toxin isoforms), exendin, CRiSP,[1] kallikrein, natriuretic peptides, and type III phospholipase A_2 (4, 20, 22). Two of these (CRiSP and kallikrein) are homologous to forms found in snake venoms (4, 18, 19, 23). An additional toxin type (helokinestatin peptides) are not the result of a recruitment event but rather are unique proline-rich derivatives within the ancestral gene (located upstream from the natriuretic peptide-encoding region) that are post-translationally cleaved off to form discrete bioactive

[1] The abbreviations used are: CRiSP, cysteine-rich secretory protein; BLAST, basic local alignment search tool; RACE, rapid amplification of cDNA ends; CCK, cholecystokinin; T, tesla; PLA_2, phospholipase A_2; CRD, carbohydrate recognition domain; BNP, brain natriuretic peptide; CNP, C-type natriuretic peptide; VIP, vasoactive intestinal peptide.

peptides (22, 24). Helokinestatin peptides are thus a rare case of a single gene being mutated to additionally encode multiple products. Helokinestatin peptides are thus far known only from *Heloderma* venoms, and the two varanid natriuretic precursor sequences reported to-date lack these derivatives (4, 20, 22).

As the venoms of Anguimorpha lizards have received less attention than those of the more medically important venomous snakes, it remains unknown to what extent the different toxin types have diversified and undergone structural and functional innovation. Detailed knowledge of the anguimorph toxins therefore is crucial for insight into the structure, function, and composition of the ancestral Toxicofera venom system and to address the question of how multiple lineages achieved evolutionary innovations. A thorough understanding of the molecular and functional diversity is also necessary to fully exploit the therapeutic potential of these venoms.

Transcriptome analyses by random sequencing of cDNA libraries has been proven to be an effective way of identifying novel isoforms of previously reported toxins as well as toxins of new protein classes (see Refs. 4, 18, 20, 22, 25, and 26), thus providing new insights into the molecular evolutionary origins. In this study, we have integrated multidisciplinary data to provide an in-depth investigation of anguimorph lizard venom molecular evolution to (*a*) characterize the venom transcriptomes of representative anguimorph lizards, (*b*) determine the timing of toxin recruitment events and patterns of toxin diversification, and (*c*) characterize changes in the venom gland structure and delivery architecture.

MATERIALS AND METHODS

Species Examined

Adult stage specimens of the following species were examined by either construction of a mandibular venom gland cDNA library (C), histology (H), or magnetic resonance imaging (M) as noted: Anguidae *Celestus warreni* (Haiti) (C, H, and M), *Gerrhonotus infernalis* (Texas) (C, H, and M), and *Ophisaurus apodus* (Greece) (C, H, and M); Helodermatidae *Heloderma horridum horridum* (captive-bred offspring of founder stock from unknown geographical origin) and *Heloderma suspectum cinctum* (captive-bred offspring of founder stock from unknown geographical origin) (C and M); Lanthanotidae *Lanthanotus borneensis* (Borneo) (M); Shinisauridae *Shinisaurus crocodilurus* (captive-bred offspring of founder stock from unknown geographical origin) (H); and Varanidae *Varanus acanthurus* (Newman, Western Australia) (C and M), *Varanus albigularis* (captive-bred offspring of founder stock from unknown geographical origin) (M), *Varanus eremius* (Giralia Station, Western Australia) (C), *V. giganteus* (Sandstone, Western Australia) (C and M), *Varanus gilleni* (captive-bred offspring of founder stock from unknown geographical origin) (C and M), *Varanus glauerti* (Kununurra, Western Australia) (C), *Varanus gouldii* (Kununurra, Western Australia) (C and M), *Varanus indicus* (Alligator River, Northern Territory, Australia) (C), *V. komodoensis* (captive-bred offspring of founder stock from unknown geographical origin) (C, H, and M), *Varanus mertensi* (Kununurra, Western Australia) (C and M), *Varanus mitchelli* (Kununurra, Western Australia) (M), *Varanus panoptes panoptes* (Kununurra, Western Australia) (C and M), *Varanus prasinus* (captive-bred offspring of founder stock from unknown geographical origin) (M), *Varanus salvator* (Bali, Indonesia) (M), *Varanus scalaris* (Kununurra, Western Australia) (C and M), *Varanus tristis orientalis* (captive-bred offspring of founder stock from unknown geographical origin) (C and M), and *Varanus varius* (Mallacoota, Victoria, Australia) (C and H). Different individuals were used for each method.

cDNA Library Construction and Analysis

To investigate the relationship between toxins and the encoding transcripts and also facilitate molecular evolutionary analyses, venom gland cDNA libraries were constructed from glands that had been surgically excised from living specimens under general anesthesia and immediately cryogenically preserved. RNA was harvested using the Qiagen RNeasy Midi kit with subsequent selection of mRNAs using the Oligotex Midi kit. cDNA libraries were constructed using the Clontech Creator SMART cDNA Library Construction kit and transformed into One Shot Electrocompetent GeneHogs (Invitrogen). Isolation and sequencing of inserts was conducted at the Australian Genome Research Facility using BDTv3.1 chemistry with electrophoretic separation on an AB330xl. 384 colonies were sequenced, inserts were screened for vector sequences, and those parts were removed prior to analysis and identification.

Toxin sequences were identified by comparison of the translated DNA sequences with previously characterized toxins using a BLAST search of the Swiss-Prot/UniProt protein database (http://www.expasy.org/tools/blast/). In sequence alignments, signal peptides were ascertained utilizing the SignalP 3.0 Server (http://www.cbs.dtu.dk/services/SignalP/). Molecular phylogenetic analyses of toxin transcripts were conducted using the translated amino acid sequences. Comparative sequences from other venomous reptiles and outgroups were obtained through BLAST searching (http://www.expasy.org/tools/blast/) using representative toxin sequences. To minimize confusion, all sequences obtained in this study are referred to by their GenBank™ accession numbers (http://www.ncbi.nlm.nih.gov/sites/entrez?db=Nucleotide), and sequences from previous studies are referred to by their UniProt/Swiss-Prot accession numbers (http://www.expasy.org/cgi-bin/sprot-search-ful) except for the previously reported snake veficolin sequences, which are referred to by their GenBank accession numbers. Resultant sequence sets were aligned using the program ClustalX followed by visual inspection for errors. When presented as sequence alignments, the leader sequence is shown in lowercase, the prepro region is underlined, cysteines are highlighted in black, and functional residues are in bold. Data sets were analyzed using Bayesian inference implemented on MrBayes, version 3.0b4. The analysis was performed by running a minimum of 1×10^6 generations in four chains and saving every 100th tree. The log likelihood score of each saved tree was plotted against the number of generations to establish the point at which the log likelihood scores of the analysis reached their asymptote, and the posterior probabilities for clades were established by constructing a majority rule consensus tree for all trees generated after the completion of the burn-in phase. Sequence alignments can be obtained by e-mailing Dr. Bryan Grieg Fry.

RT-PCR

10-mg samples of lyophilized venom from each lizard species (*H. suspectum* and *H. horridum*) were dissolved separately in 1 ml of cell lysis/mRNA protection buffer supplied by Dynal Biotech. Polyadenylated mRNA was isolated by the use of magnetic oligo(dT) beads as described by the manufacturer (Dynal Biotech). mRNA was eluted in 20 μl of RNase-free water, and first strand cDNA synthesis for subsequent RACE reactions was performed using a SMART-RACE kit (Clontech) essentially as described by the manufacturer. Exendin RACE reactions were amplified using two sets of sense primers (S1, ATGAAAATCATCCTTTGGCTGTGTGTTT; S2, ATGAAAAGCATC-

CCTGTCAGCTGGCAAATGGCT) and antisense primers (AS1, CGATGGCGGCCTTGGTGATGTT; AS2, TAACGCGATGGCGGAGGTGGT) for the cDNAs by thermostable polymerase (Invitrogen). These primers were complementary (S1/AS1) or partially complementary (S2/AS2) to a domain of nucleotide sequences in the 5′ and 3′ regions of the exendin-2 precursor cDNA cloned previously (*H. suspectum cinctum* (GenBank accession number EU790760). The PCR cycling procedure was as follows: an initial denaturation step for 1 min at 94 °C followed by 35 cycles consisting of denaturation for 30 s at 94 °C, primer annealing for 30 s at 62 °C (S1/AS1) or 58 °C (S2/AS2), and extension for 3 min at 72 °C. Gel electrophoresis of the PCR products from the venom library of each species was followed by further purification, cloning using a pGEM-T vector system (Promega Corp.), and subsequent sequencing using an ABI 3100 automated capillary sequencer. Kallikrein RACE reactions were amplified using two sets of sense primers (S1, ATCATTGGAGGCCAGGAATGCCCCC; S2, ATCATTGGAGGCCAGGAATGCC) and antisense primers (AS1, GCCCGGCTCCAATGGCTGAG; AS2, GAACAAGGTGAAAAATATGGT) for the cDNAs by thermostable polymerase (Invitrogen). These primers were complementary to 5′ and 3′ regions of the precursor cDNA EU790962 cloned from *H. suspectum cinctum* in this study (S1/AS1) and backward translations of the protein sequence P43685 reported previously from *H. horridum* (S2/AS2) (34). The PCR cycling procedure was as follows: an initial denaturation step for 1 min at 94 °C followed by 35 cycles consisting of denaturation for 30 s at 94 °C, primer annealing for 30 s at 62 °C, and extension for 3 min at 72 °C. Gel electrophoresis of the PCR products from the venom library of each species was followed by further purification, cloning using a pGEM-T vector system (Promega Corp.), and subsequent sequencing using an ABI 3100 automated capillary sequencer.

Bioactivity Characterization of Cholecystoxin, Celestoxin, Goannatyrotoxin, Helokinestatin, Natriuretic, and YY Peptides

Peptide Synthesis—Peptides were synthesized on a CEM Liberty Peptide Synthesizer using Fmoc (*N*-(9-fluorenyl)methoxycarbonyl) solid-phase peptide chemistry. The peptides were cleaved from the solid-phase resin with TFA/H_2O/triisopropylsilane/3,6-dioxa-1,8-octanedithiol (90:2.5:2.5:5) for 2 h. The crude peptides were isolated by ether precipitation, dissolved in 30:70 (v/v) ACN/H_2O, and lyophilized. The crude linear peptides were reversed-phase HPLC-purified (Agilent 1200 HPLC System) before forming the single disulfide bond (in the natriuretic peptide only) by treatment with dipyridyldithiol (1 eq) in 100 mM ammonium acetate (peptide concentration, 1 mg/ml; 30 min). The pure cyclized natriuretic peptide was isolated by directly applying the ammonium acetate solution to a reversed-phase HPLC column, isolating pure peptide fractions, and lyophilization of the products. The identity of the pure cyclized peptide was confirmed by high resolution mass spectrometry on an Agilent Q-TOF 6510 LC/MS mass spectrometer.

Anesthetized Rat Studies—Male Sprague-Dawley rats were anesthetized with pentobarbitone sodium (60–100 mg/kg intraperitoneally). A midline incision was made in the cervical region, and cannulas were inserted into the trachea, jugular vein, and carotid artery for artificial respiration (if required), administration of peptides, and measurement of blood pressure, respectively. Arterial blood pressure was recorded using a Gould P23 pressure transducer connected to a PowerLab system. All results were expressed as change in mean arterial pressure.

Guinea Pig Isolated Ileum Studies—Guinea pigs of either sex were killed by CO_2 inhalation and exsanguination. The ileum was removed and cut into 2-cm segments. Segments of ileum were then mounted on wire tissue holders under 1-g resting tension in 5-ml organ baths containing physiological salt solution of the following composition: 118.4 mM NaCl, 4.7 mM KCl, 1.2 mM $MgSO_4$, 1.2 mM KH_2PO_4, 25.0 mM $NaHCO_3$, 11.1 mM glucose, 2.5 mM $CaCl_2$ continuously bubbled with carbogen (95% O_2, 5% CO_2) and maintained at 34 °C. The preparation was allowed to equilibrate for 30 min. A cumulative concentration-response curve to bradykinin (1 nM–1 μM) using half-log unit increments was then obtained. The peptide (0.1 μM) was then added and left to equilibrate for 30 min. A cumulative concentration-response curve to bradykinin (1 nM–1 μM) was then repeated in the presence of the peptide as described above. Isometric contractions were measured via a Grass force displacement transducer (FT03) and recorded using a PowerLab system. Responses to bradykinin in the presence of the peptide were expressed as a percentage of the maximum response obtained from the initial bradykinin curve.

Rat Isolated Aorta—Male Sprague-Dawley rats were killed by CO_2 inhalation and exsanguination. The thoracic aorta was removed, cleaned of surrounding connective tissue, and cut into 5-mm rings. Aortic rings were mounted in organ baths containing physiological solution (as above). The aortic rings were maintained at 37 °C and suspended between wire hooks at a resting tension of 10 g. Isometric contractions were measured by a Grass force displacement transducer (FT03) and recorded using a PowerLab. Tissues were precontracted with phenylephrine (10 mM), and at the plateau of contraction, relaxation responses to peptides were obtained.

Cholecystokinin (CCK) Receptor Binding—The source of Type 1 (or Type A). As previously described (70) the CCK receptor utilized in these studies was the Chinese hamster ovary cell line expressing the wild type rat receptor (CHO-CCKR) and particulate preparation enriched in plasma membranes was prepared from these cells. This involved non-enzymatic lifting of the cells, homogenization, and separation of cellular fractions on a sucrose gradient. Membranes were suspended in Krebs-Ringer-HEPES medium (25 mM HEPES at pH 7.4, 104 mM NaCl, 5 mM KCl, 1 mM KH_2PO_4, 2 mM $CaCl_2$, 1.2 mM $MgSO_4$) supplemented with 1 mM phenylmethylsulfonyl fluoride (PMSF) and 0.01% soybean trypsin inhibitor. Binding activity was evaluated in standard competition binding assays utilizing radioiodinated CCK analog (^{125}I-D-Tyr-Gly-[(Nle^{28,31})CCK(26–33)] where Nle is norleucine) as the radioligand (specific radioactivity, 2000 Ci/mmol). Cell membranes containing 5–10 μg of protein were incubated with 10 pM radioligand (~20,000 cpm) in a volume of 0.5 ml of Krebs-Ringer-HEPES medium containing 0.2% bovine serum albumin and 0.01% soybean trypsin inhibitor in the presence of increasing concentrations of non-radioactive ligand (0–1 μM). Incubations were performed for 1 h at room temperature to achieve saturable binding. Rapid separation of bound from free radioligand was achieved with a Skatron cell harvester (Molecular Devices, Sunnyvale, CA) equipped with receptor-binding filter mats. Bound radioactivity was quantified in a γ-spectrometer. Non-saturable binding was determined in the presence of 1 μM unlabeled human CCK8 and represented less than 25% of total cpm bound in each case. Data were graphed using Prism version 3.0 (GraphPad Software, San Diego, CA) and were analyzed using the nonlinear least squares curve-fitting program LIGAND. All assays were performed in duplicate in at least three independent experiments.

Venom Gland Structural Characterization

Histological sections were prepared from the intact head and the excised venom gland and delivery system. Whole heads were removed, and a cut was made to the underside to allow fast penetration of the fixative (10% neutral buffered formalin). After a minimum of 2 days, excess tissue was removed, and specimens were immersed in Kristensen's decalcification solution and placed on a rotor for up to 3 weeks (depending on the size of the head). Before processing, the heads were bisected longitudinally for cutting transversely at 3 μm in two separate blocks. The processing schedule was as follows: 10% formalin, 2 h; absolute ethanol, 4 × 1 h; histolene, 3 × 1 h; paraffin

wax, 2 × 90 min. The sections were taken every 100 μm, and matching sections were stained with periodic acid-Schiff's stain and Masson's trichrome stain. In other specimens, the venom gland, venom duct, and adjacent bony and muscular tissues were excised and placed in decalcifying solution (Cal-Ex, Fisher) for 72–168 h. Each sample was dehydrated and cleared through a progressive ethanol series and Cyto-Sol (Fisher) prior to embedding in Paraplast (Fisher). Serial sections were cut at 10–12 μm. All species were sectioned in the frontal plane; when available, the contralateral venom gland and delivery system were sectioned either parasagittally or transversely. Sections were stained using a variant of Van Gieson's stain, which provides clear distinction between connective tissue, muscle, and epithelium, or with hematoxylin and eosin.

Magnetic resonance imaging (MRI) was used to examine the three-dimensional shape and internal anatomy of the venom glands from individual specimens of each species. For all except *Heloderma*, formalin-ethanol-fixed heads were first submersed in Fomblin (Solvay Solexis) and placed under vacuum to prevent air artifacts. Depending on head size, imaging was performed on either 9.4-tesla (T) (small/medium) or 17.6-T (large) vertical 89-mm-bore systems (Bruker BioSpin, Rheinstetten, Germany) with a Bruker Micro2.5 gradient system of 1 T/m and a transmit/receive birdcage radiofrequency coil with a diameter of 10–30 mm. Bruker ParaVision 4.0 software was used for image acquisition. Anatomical images were acquired using a three-dimensional gradient echo sequence. The field of view and matrix were varied to fit the individual samples, resulting in voxel sizes between 40^3 and 70^3 mm^3. Imaging parameters were as follows: echo time, 8 ms; repetition time, 40 ms; flip angle, 20°; 4–8 averages; total scan time, between 3 and 9 h/sample depending on size and resolution. A Philips Achieva, 1.5-T clinical MRI scanner (Philips Healthcare, Best, The Netherlands) using a surface coil with a diameter of 47 mm was used to scan the preserved heads of *H. horridum horridum* (CAS91897) and *Heloderma suspectum suspectum* (CAS34292) from the California Academy of Science. Several scout images were performed, and the coil was repositioned to obtain maximum signal to noise in the anatomical area to be imaged. A three-dimensional T2-weighted turbo spin echo sequence was acquired with the following parameters: echo train length, 11; repetition time/echo time/flip angle, 1000 ms/65 ms/90°; field of view, 100 mm; 220 slices; acquisition voxel size, 0.2 × 0.2 × 0.2 mm^3; number of signal averages, 1; scan time, 65 min (1:05:27). Images with different angulations were reconstructed afterward on a Vitrea work station (Vital Images Inc., Minnetonka, MN). Image segmentation of the glands was performed manually in Amira 4.1 (Mercury Computer Systems), and three-dimensional surface renderings were generated.

RESULTS

Toxin Transcript Types Recovered—BLAST analyses of transcripts recovered from the venom gland cDNA libraries identified seven protein types with sequence homology to previously characterized toxicoferan toxins (Table I). Three toxin types previously only sequenced from snake venoms were recovered in this study: lectin (recovered from *O. apodus* and *V. indicus*), hyaluronidase (recovered from *H. suspectum cinctum* and *G. infernalis*), and veficolin (*V. komodoensis*). CRiSP, kallikrein, natriuretic peptide, and PLA_2 transcripts were sequenced for the first time from anguid lizards, and additional isoforms were sequenced from the helodermatid and varanid libraries. Nerve growth factor was sequenced for the first time from *Heloderma.* Similar to the multidomain-encoding transcripts from *Heloderma*, homologous anguid natriuretic mRNA full-length transcripts also were multidomain-, multiproduct-encoding (natriuretic and helokinestatin peptides). However, the characteristic helokinestatin proline-rich domains remained consistently absent from the varanid natriuretic transcripts (Fig. 2*A*). Although exendin-3 and -4 are present in large amounts in both *Heloderma* species and easily purified by reversed-phase HPLC, in contrast, exendin-1 and -2 peaks were only visible in *H. suspectum.* Specific primer-directed PCR studies showed strong levels of exendin-1 in *H. suspectum*, but trace amounts were detected in *H. horridum* (Fig. 3*A*). In contrast, exendin-2 was also strongly detected in *H. suspectum* but entirely absent from *H. horridum* (Fig. 3*B*).

Toxin Molecular Evolution—The CRiSP toxins showed differential variation in structural and functional domains, particularly in the residues that guide bioactivity (Fig. 4). The cysteine pattern and other structural residues were highly conserved as was the PR1 tetrad functional domain. However, the PR1 binding site displayed a much lower level of conservation. Similarly, the ion channel-binding residues in the CRD were also quite variable. In two variants, newly evolved cysteines were present: one in the *C. warreni* isoform GU441473 upstream from the first ancestral cysteine and the other one in between the second and third ancestral cysteines of the two isoforms recovered from *V. indicus* (GU441469 and GU441470). Both *V. indicus* isoforms were also truncated, lacking the last six cysteines.

Newly evolved cysteines were also shown to be present in two different kallikrein variants: one type from the anguid clade and two others from the varanids (Fig. 5). In a novel form of the kallikrein toxins recovered from both the *C. warreni* and *G. infernalis* libraries, there was not only a newly derived cysteine at alignment position 219 but also a deletion of the last ancestral cysteine. In the variant recovered from both the *V. acanthurus* and *V. scalaris* libraries, a new cysteine was evolved at alignment position 124, resulting in an odd number of cysteines.

A long C-terminal tail was revealed in the protein translations of the *H. suspectum* PLA_2 mRNA sequences in this study that had not been seen in either of the reported *H. suspectum* sequences previously determined by protein sequencing (P80003 and P16354) (Fig. 6). The translated forms of the full-length mRNA sequences corresponding to the region at which the protein sequences stop (Gly for P80003 and GR for P16354) are rich in dibasic proteolytic sites (GRKRSQKKRK for EU790967 and GRKRSRKKRK for EU790968) (Fig. 6), common recognition sites for proteolytic removal of segments in precursors from both vertebrates (27) and invertebrates (28). Therefore, P16354 may represent an incompletely proteolyzed product relative to P80003. The C-terminal tail of EU790968 is much longer than that of EU790967, which terminates with the proteolysis motif. The full-length sequences from the anguids and varanids revealed that this RK proteolytic cleavage motif is ubiquitously present in anguimorph isoforms and thus represents a basal condition (Fig. 6).

TABLE I

Anguimorpha lizard mandibular venom gland mRNA sequences recovered in this study that are homologous to previously characterized Toxicofera toxins

GC-A, guanylyl cyclase A.

Toxin type	Species	GenBank accession no.	Bioactivity
CRiSP	All	EU790958, GU441462, GU441463, GU441464, GU441465, GU441466, GU441467, GU441468, GU441469, GU441470, GU441471, GU441472, GU441473	Blockage of ryanodine receptors and potassium channels, producing lethargy, paralysis, and hypothermia (57–61)
Helokinestatin	*C. warreni*, *G. infernalis*	GU441510, GU441511	Bradykinin inhibition (22, 24); bioactivity determined for new variants from anguid venoms in this study (Fig. 2*D*).
Hyaluronidase	*G. infernalis*, *H. suspectum*	EU790961, GU441476	Venom spreading factor (42)
Kallikrein	All	EU790962, GU441477, GU441478, GU441479, GU441480, GU441481, GU441482, GU441483, GU441484, GU441485, GU441486, GU441487, GU441488, GU441489, GU441490, GU441491, GU441492, GU441493, GU441494, GU441495, GU441496, GU441497, GU441498, GU441499, GU441500, GU441501, GU441502, GU441503, GU441504, HM437246	Release of bradykinin from kinogen (34, 62–65); a derivative form also cleaves fibrinogen (66)
Lectin	*O. apodus*, *V. indicus*	GU441505, GU441506	Snake venom forms have been shown to have various modes of action upon platelet aggregation (67, 68)
Natriuretic peptide	*C. warreni*, *G. infernalis*, *H. suspectum*, *V. glauerti*, *V. scalaris*	EU790965, GU441507, GU441508, GU441509, GU441510, GU441511	Hypotension induction leading to loss of consciousness; mediated through the binding of GC-A, resulting in the relaxation of cardiac smooth muscle (4, 16, 20); structure-function studies in this study revealed residues crucial for bioactivity (Fig. 2, *B* and *C*)
Nerve growth factor	*H. suspectum cinctum*	EU790966	Uncharacterized
PLA_2	*C. warreni*, *H. suspectum*, *V. gilleni*, *V. glauerti*, *V. scalaris*, *V. tristis*	EU790967, EU790968, GU441524, GU441525, GU441526, GU441527, GU441528,	Inhibition of epinephrine-induced platelet aggregation (4, 69)
Veficolin	*V. komodoensis*	HM641898	Uncharacterized

Phylogenetic analysis of the lizard venom natriuretic peptides showed them to be the result of an independent toxin recruitment event relative to the natriuretic peptides from snakes venoms (Fig. 7). Each lineage formed a monophyletic group that was reciprocally monophyletic, all lizard toxins clustering together and all snake toxins clustering together but with the two toxin types being phylogenetically distinct from each other. Consistent with the lack of atrial natriuretic peptide in the reptile physiology (29), the lizard venom types were nested within the BNP clade. In contrast, as reported previously (30), the snake forms were all nested within the CNP clade (Fig. 7). The ASDEN sequence that links the *Heloderma* post-translationally cleaved helokinestatin peptide isoforms encoded by the multidomain, multiproduct natriuretic transcript (22) was only partially conserved between variants in *G. infernalis* (AAEEN, AEEN, and AEGEEN), respectively) but not at all conserved in the same proline-rich region of the *C. warreni* transcript (Fig. 2*A*). In contrast, phylogenetic analysis showed the lizard and snake veficolin sequences to form a monophyletic group with high statistical support, and

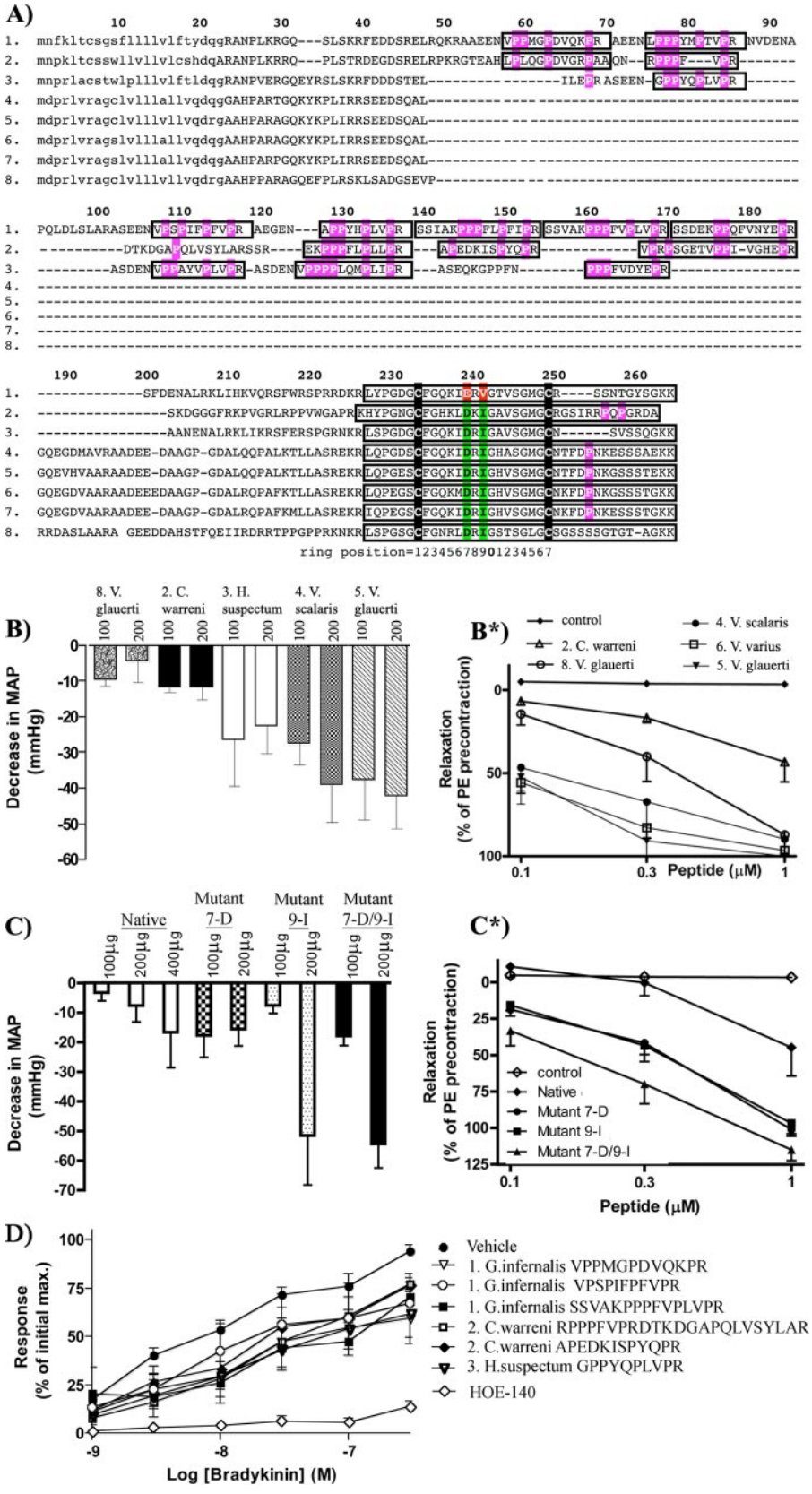

FIG. 2. *A*, alignment of natriuretic peptide/helokinestatin-encoding precursors from the mandibular venom glands of *G. infernalis* (GU441510) (*1*), *C. warreni* (GU441511) (*2*), *H. suspectum cinctum* (EU790965) (*3*), *V. scalaris* (GU441508) (*4*), *V. glauerti* (GU441509) (*5*), *V. varius* (Q2XXL8) (*6*), *V. komodoensis* (B6CJV0) (*7*), and *V. glauerti* (GU441509) (*8*). Bounding *boxes* surround post-translationally cleaved bioactive peptides, functionally important prolines are highlighted in *magenta*, cysteines are in *black*, and two typically invariant natriuretic peptide intraring residues (Asp_7 and Ile_9) are in *green*. The signal sequence is in *lowercase*. *B*, Effect of post-translationally cleaved bioactive natriuretic peptide isoforms on (*B*) mean arterial pressure or (*B**) endothelium denuded aortic ring. *C*, structure-function relationships of a natriuretic peptide variant from *G. infernalis* that lacks the two invariant amino acids Asp_7 (*7-D*) and Ile_9 (*9-I*) on (*C*) mean arterial pressure or (*C**) endothelium denuded aortic ring. *D*, effect of helokinestatin peptides (0.1 mM; *n*_5) on cumulative concentration-response curves to bradykinin (1 nM–0.3 mM); peptide sequence tested follows each taxon name. *NP*, natriuretic peptide; *PE*, phenylephrine. In panels *B* and *D*, number before each taxon identifies in *A* the precursor of the peptide being tested.

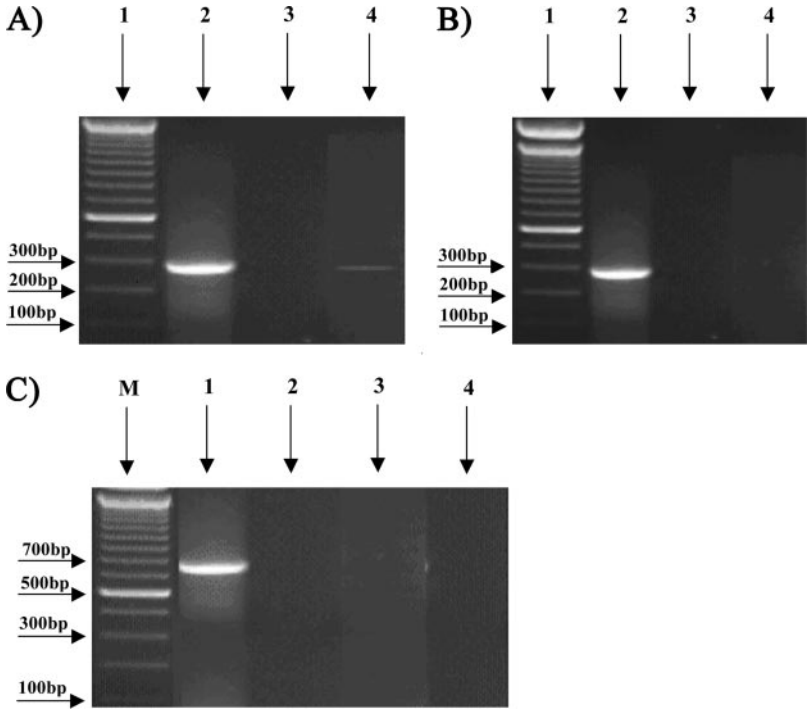

FIG. 3. Gel electropherograms of RT-PCR products generated from gene-specific primers for exendin-1 (*A*) and exendin-2 (*B*) are shown. *Lane 1*, standard DNA ladder, each band representing 100-base pair increments; *lane 2*, RT-PCR product from the venom library of *H. suspectum*; *lane 3*, non-template control; *lane 4*, RT-PCR from venom libraries of Mexican beaded lizard (*H. horridum*). *C*, gel electropherogram of RT-PCR products generated from kallikrein gene-specific primers. *Lane M*, standard DNA ladder, each band representing 100-base pair increments; *lane 1*, RT-PCR product from the venom library of *H. horridum* with primers designed from *H. suspectum* kallikrein sequence EU790962 obtained in this study; *lane 2*, non-template control; *lane 3*, RT-PCR from venom libraries of *H. horridum* with primers designed from the *H. horridum* kallikrein sequence P43685 reported previously; *lane 4*, non-template control.

thus this toxin type is another core toxicoferan recruitment (Fig. 8).

Bioactivity Testing—The natriuretic peptides were shown to be variable in cardioactivity (Fig. 2, *B* and *C*), ranging from weakly active (GU441511 from *C. warreni*, GU441510 from *G. infernalis*, and GU441509 from *V. glauerti*) to as equipotent as previously studied variants (EU790965 from *H. suspectum*, GU441507 from *V. glauerti*, and GU441508 from *V. scalaris*) from other anguimorph lizards (4, 20) or from snakes (16). GU441510 from *G. infernalis* lacked two intraring invariant amino acids, and residue replacement studies demonstrated that both contribute equally to bioactivity (Fig. 2*C*). Bioactivity testing of representative taxonomical samplings of helokinestatin variants also encoded by the natriuretic gene demonstrated variable contractile inhibiting responses to bradykinin in the guinea pig ileum (Fig. 2*D*).

Characterization of Novel Toxin Classes—Three new peptide toxin types (cholecystoxin, goannatyrotoxin, and celestoxin) were discovered, and bioactivity was characterized (Table II and Figs. 9–11). All three peptides lacked cysteines with goannatyrotoxin and celestoxin having secondary structure determined by significant numbers of prolines. Cholecystoxin (GU441461), recovered from the *V. varius* library, was homologous to cholecystokinin peptides normally expressed in a myriad of tissue types (Fig. 9*A*). Analog testing elucidated that the smallest sized cleavage fragment with full cardiovascular activity and receptor CCK-A binding activity was an octapeptide domain seen in normal body cholecystokinin peptides (Fig. 9*B*). However, testing also demonstrated that a sulfated tyrosine was crucial for activity with even a phosphotyrosine analog ineffective in receptor binding (Fig. 9*B*). Goannatyrotoxin (GU441529), recovered from the *V. eremius* library, was homologous to YY peptides normally expressed in the intestine (Fig. 10*A*). Bioactivity testing revealed a potent unique triphasic action, rapid biphasic hypertension followed by prolonged hypotension (Fig. 10, *B* and *C*). The third type, celestoxin, recovered from *C. warreni*, did not show any significant homology to any known protein type ($E < 10$) (Fig. 11). Two isoforms (GU441474 and GU441475) that differed only in a 12-amino acid insertion at alignment positions 135–147 were recovered. Both peptides had an arginine-rich cleavage motif to liberate the bioactive domain from the propeptide (Fig. 11). Contained within the bioactive domain was a sequence repeat (ALGVVGGLPVPK and LPGVAGGLPVPK) that differed crucially in the formation of a proline bracket missing in the first repeat that has a Leu residue in place of the Pro residue. Celestoxin analog testing revealed that this internal proline-bracketed motif LPGVAGGLPVPK is responsible for full activity with the activity of this fragment being equipotent to the activity of the full-length peptide in producing hypotension, whereas the ALGVVGGLPVPK fragment was inactive. Neither adrenoreceptor antagonists nor 5-hydroxytryptamine antagonists could prevent or reverse the response.

In addition to the three peptide types characterized above, also recovered were mutant versions of the epididymal secretory protein and ribonuclease molecular scaffolds (Table II), each displaying evidence of the typical toxin-characteristic duplication and diversification (Figs. 12 and 13). The epididymal secretory protein sequences recovered from the libraries of three varanids were notable in being significantly longer than corresponding normal body proteins, including an additional eight cysteines (Fig. 12). Within these venom gland

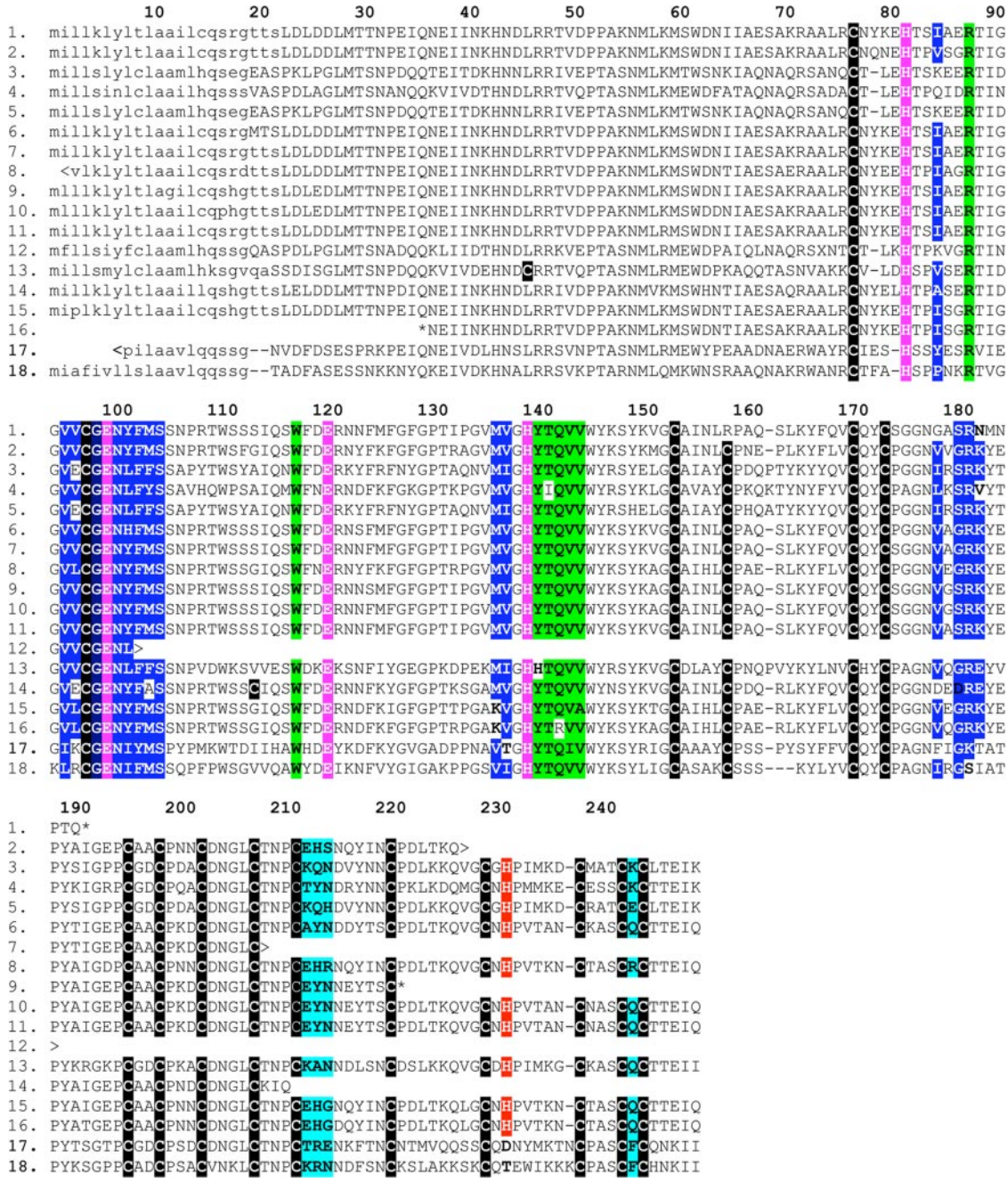

FIG. 4. **Sequence alignment of CRiSP toxins from mandibular venom glands (*1–16*) and related toxins from maxillary venom glands of snakes (*17* and *18*).** *1*, *Varanus giganteus* (GU441466); *2*, *V. acanthurus* (Q2XXR0); *3*, *H. horridum* (Q91055); *4*, *G. infernalis* (GU441472); *5*, *H. suspectum cinctum* (EU790958); *6*, *V. varius* (Q2XXP1); *7*, *V. komodoensis* (B6CJU4); *8*, *V. gilleni* (GU441467); *9*, *V. panoptes* (GU441464); *10*, *V. gouldii* (GU441465); *11*, *V. mertensi* (GU441463); *12*, *O. apodus* (GU441462); *13*, *C. warreni* (GU441473); *14*, *V. indicus* (GU441469); *15*, *V. tristis* (GU441468); *16*, *V. scalaris* (GU441471); *17*, *T. stejnegeri* (P60623); *18*, *P. australis* (Q8AVA4). Highlighted sequences correspond to PR1 tetrad (*magenta*), PR1 structurally important residues (*green*), PR1 substrate binding site (*dark blue*), CRD possible ion channel blocking sites (*light blue*), cysteines (*black*), and otherwise unassigned conserved surface histidines (*red*). The signal sequence is in *lowercase*. < and > designate incomplete N and C termini of the precursor, respectively. * designates the N terminus of a post-translationally processed protein sequence.

isoforms, two variant classes were present that differed in a deletion in alignment positions 115–157 that removes four of the 20 cysteines (Fig. 12) with potential resultant consequences for structure and function. The ribonuclease sequences from *G. infernalis* lack two of the ancestral cysteines present in the normal body form (Fig. 13). Two of these isoforms had a frameshift mutation near the C terminus, resulting not only in slightly truncated sequences and the loss of

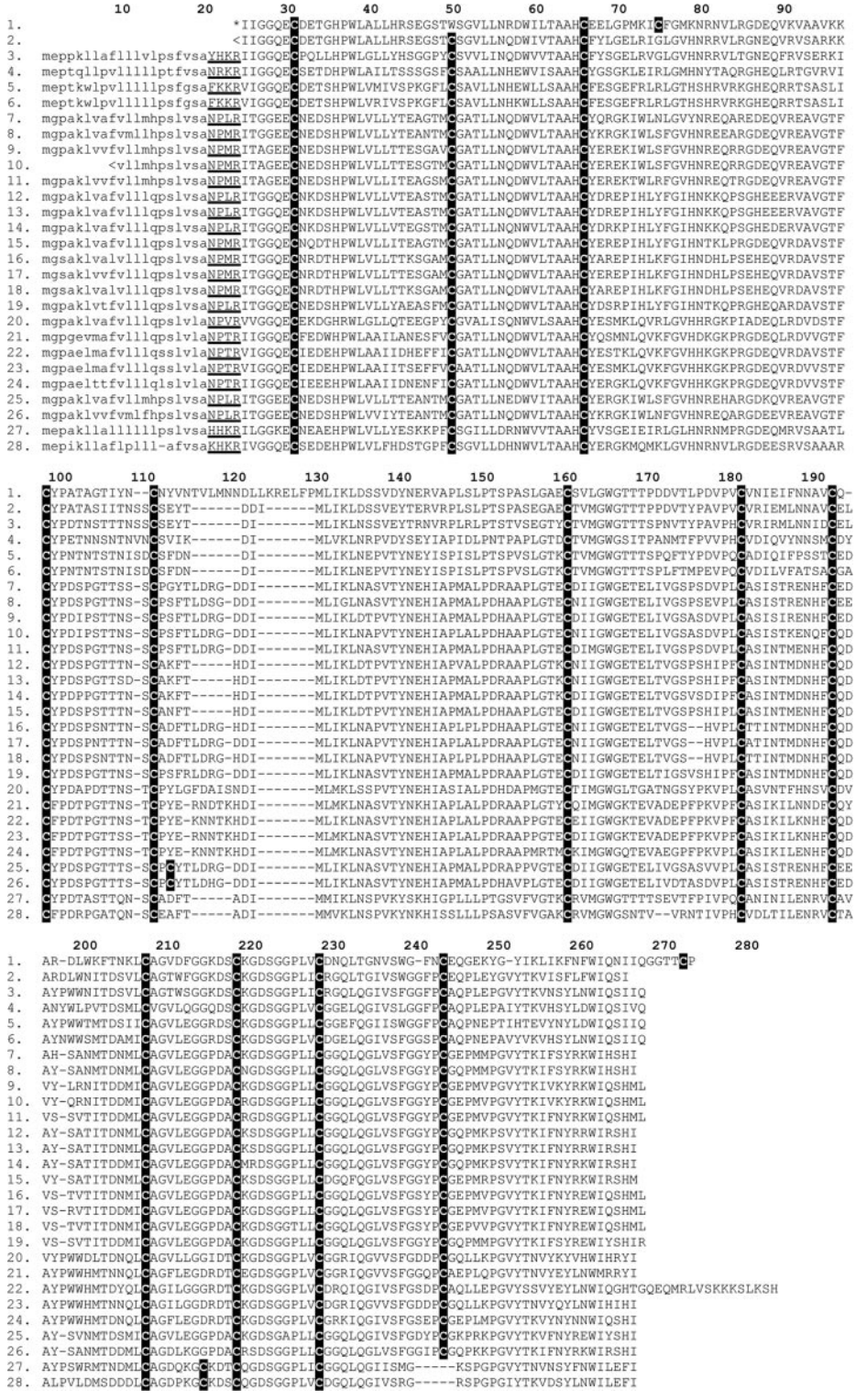

FIG. 5. **Sequence alignment of kallikrein toxins from mandibular venom glands.** *1*, *H. horridum* (P43685) sequenced previously (34); *2*, *H. horridum* sequenced in this study (HM437246); *3*, *H. suspectum* (EU790962); *4*, *G. infernalis* (GU441495); *5*, *C. warreni* (GU441497); *6*, *C. warreni* (GU441498); *7*, *V. glauerti* (GU441481); *8*, *V. gilleni* (GU441480); *9*, *V. gouldii* (GU441483); *10*, *V. panoptes* (GU441490); *11*, *V. mertensi* (GU441484); *12*, *V. glauerti* (GU441487); *13*, *V. tristis* (GU441488); *14*, *V. scalaris* (GU441491); *15*, *V. indicus* (GU441482); *16*, *V. gouldii* (GU441489); *17*, *V. gouldii* (GU441485); *18*, *V. gouldii* (GU441492); *19*, *V. mitchelli* (Q2XXN0); *20*, *V. komodoensis* (B6CJU6); *21*, *V. scalaris* (VSCA_CL3Contig1); *22*, *V. gouldii* (GU441478); *23*, *V. komodoensis* (B6CJU5); *24*, *V. indicus* (GU441479); *25*, *V. scalaris* (GU441486); *26*, *V. acanthurus* (Q2XXN1); *27*, *G. infernalis* (GU441496); *28*, *C. warreni* (GU441473). Cysteines are highlighted in *black*, and the signal sequence is shown in *lowercase*. The prepro region is *underlined*. < designates an incomplete N terminus of the precursor. * designates the N terminus of a post-translationally processed protein sequence.

two of the ancestral cysteines but also producing two new cysteines (Fig. 13).

Structural Variation of Venom System—The combination of MRI and histological analysis revealed extensive variations in the relative size and shape of the mandibular venom glands, the central lumina, and the associated duct system (Figs. 14 and 15). Differences were notable in both the number and physical orientation of the gland compartments as well as the relative encapsulation of the glands. The number of discernible compartments ranged from three discernible compart-

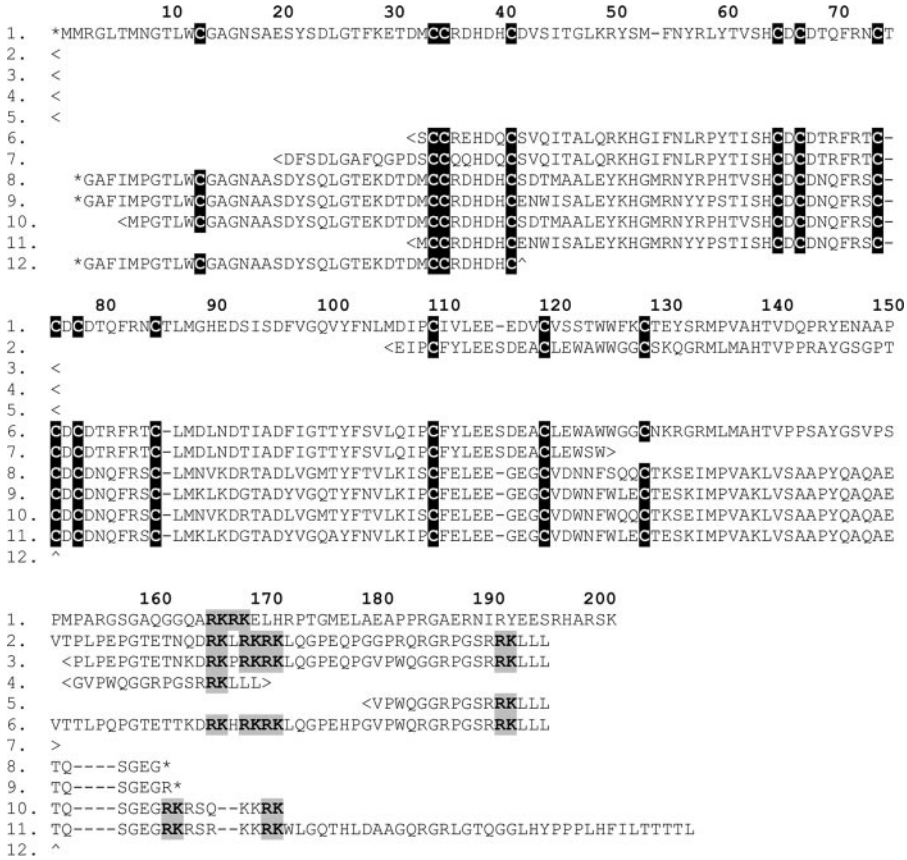

FIG. 6. **Sequence alignment of phospholipase A_2 (type III) toxin precursors from mandibular venom glands.** *1*, *C. warreni* (GU441524); *2*, *V. gilleni* (GU441524); *3*, *V. scalaris* (GU441526); *4*, *V. glauerti* (GU441527); *5*, *V. tristis* (GU441528); *6*, *V. komodoensis* (B6CJU9); *7*, *V. varius* (Q2XXL5); *8*, *H. suspectum* (P80003); *9*, *H. suspectum* (P16354); *10*, *H. suspectum* (EU790967); *11*, *H. suspectum* (EU790968); *12*, *H. horridum* (P04362). Cleavage motifs are highlighted in *gray*, cysteines are in *black*, and the signal sequence is shown in *lowercase*. < and > designate incomplete N and C termini of the precursor, respectively. * designates the N and C termini of a post-translationally processed protein sequence. ^ designates a protein sequencing fragment with an incomplete C terminus.

ments in *Lanthanotus* (Fig. 15*D*), six compartments in both *H. horridum* and *H. suspectum* (Fig. 15, *A* and *B*), and six compartments in all *Varanus* examined in this study in gland arrangements homologous to that previously shown for *V. komodoensis* (19) to one compartment per tooth for up to 16 compartments in the anguid lizards as shown for *Celestus*, *Gerrhonotus*, and *Ophisaurus* (posteriorly located were other compartments that secreted only mucus and thus were not included in the count) (Figs. 14*C* and 15*F*).

The anguid lizards all had mixed glands with a serous portion occupying the bottom of the glands and a mucous part above it, leading to the duct, which opens at the base of the teeth, as characteristic for dental glands with the entire arrangement covered by a single thin capsule (Fig. 14*C* and 15, *F*, *G*, and *H*). *G. infernalis* and *C. warreni* have glands only on the lower jaw (Figs. 14*C* and 15*D* showing *G. infernalis*; *C. warreni* (not shown) has the same arrangement). *O. apodus*, however, has retained the ancestral condition of having glands in the maxillary region and the mandibular glands (Fig. 15*C*). Although the maxillary gland is smaller than those in *Gerrhonotus* and *Celestus*, both the maxillary and mandibular glands have unstructured central lumens homologous to those seen in *Gerrhonotus* and *Celestus* mandibular glands.

Heloderma, *Lanthanotus*, and *Varanus* displayed segregated mucus and protein glands. The serous protein-secreting glands having well structured central lumens, and the entire arrangement was covered by thick capsules. In these segregated glands, the myriad mucous lobules are located dorsally and distinct from the protein glands. *S. crocodilurus* possessed mixed seromucous infralabial lobules.

DISCUSSION

Molecular Composition of Anguimorpha Venoms—In this study, sequencing of a myriad of toxin types (Table II) from all cDNA libraries indicated the common presence of complex venom transcriptomes in Anguimorpha lizards. Multiple transcripts of the majority of toxins were recovered from individual cDNA libraries with sequences thus supported by overlapping clones. Isoforms were recovered with significant variations, including changes in key functional residues and changes in the number and spacing of cysteine residues, modifications typically associated with neofunctionalization (evolution of novel bioactivities), a pattern consistent with accelerated diversification in toxin multigene families as observed in snake venoms (13, 14, 18). The kallikrein toxins in particular showed explosive gene duplication and diversification with extensive duplication events preceding speciation.

In addition to new isoforms of previously isolated and characterized toxin types, we discovered three new peptide toxin types that we have named cholecystoxin (from *V. varius*), celestoxin (from *C. warreni*), and goannatyrotoxin (from *V. glauerti*). Of particular note is that two of our new peptide toxin

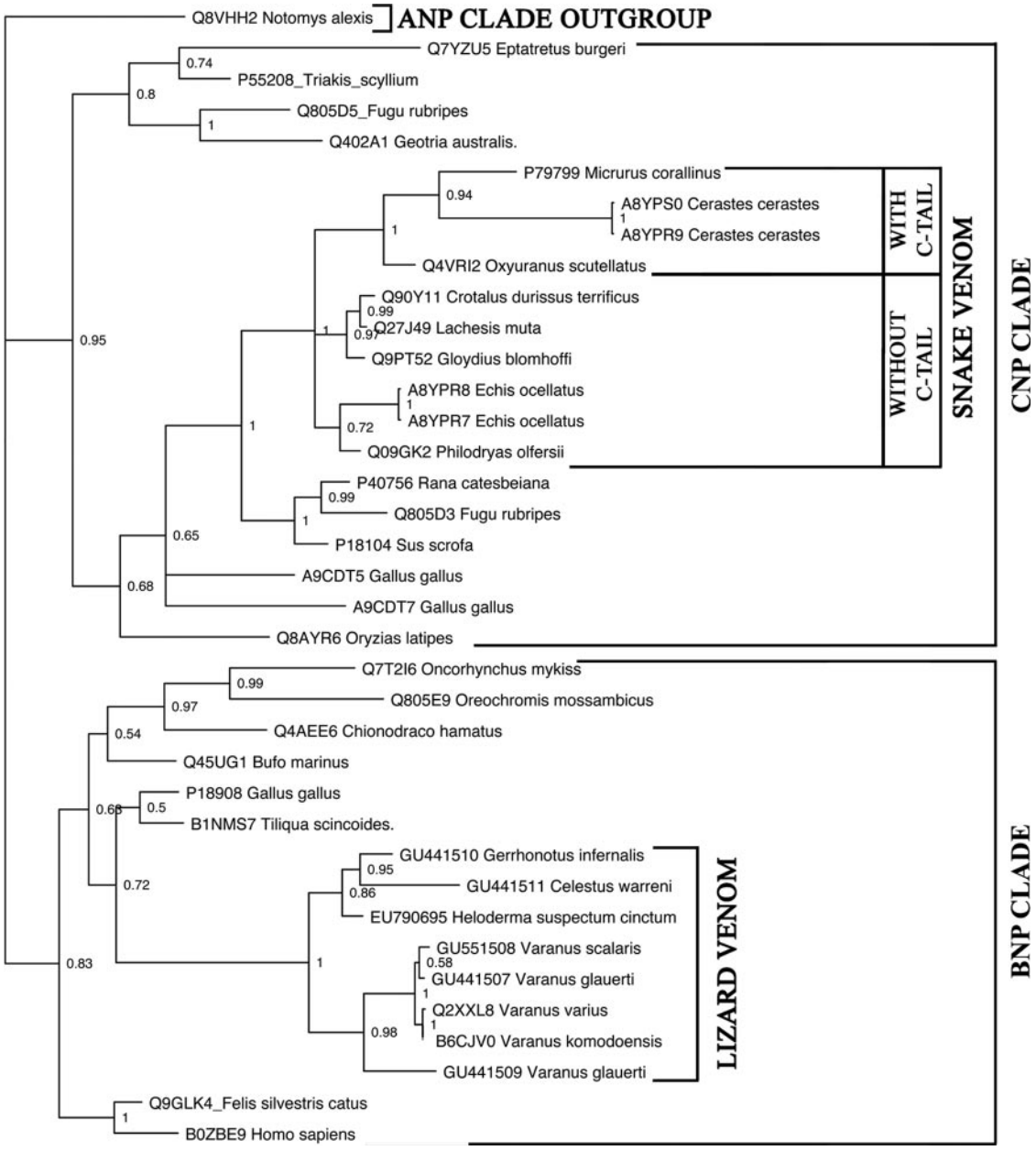

FIG. 7. **Bayesian phylogenetic reconstruction of natriuretic toxins and related non-toxin sequences.**

types (cholecystoxin and goannatyrotoxin) represent additional cases of convergence for the selection of a gene type for use as a toxin. Cholecystokinin and YY peptides have both been previously characterized as bioactive components in frog skin chemical arsenals. The cholecystokinin-derived frog peptides such as caerulein are potent ligands of CCK receptors that interfere with the physiological pathways of endogenous CCK and gastrin and cause acute pancreatitis, vomiting, diarrhea, decreased blood pressure, changes in thermoregulation, and inhibition of exploratory and feeding behaviors (31). A similar level of potency was observed for the lizard venom cholecystoxins. Endocrine effects of very low concentrations (subnanomolar) of circulating CCK are critical for nutrient homeostasis in the mammal, stimulating exocrine pancreatic secretion, gallbladder emptying, and bowel motility as well as inducing satiety. Higher concentrations of frog skin CCK-like peptides (caerulein) have been shown to stimulate pancreatic acinar cell basolateral exocytosis of zymogens central to the development of the rodent model of pancreatitis. It is interesting that CCK-like peptides secreted via the exocrine route can exhibit the toxic effects previously only attributed to a pharmacologic animal model. In contrast, although the goannatyrotoxin has a triphasic effect upon the cardiovascular system (biphasic hypertension followed by

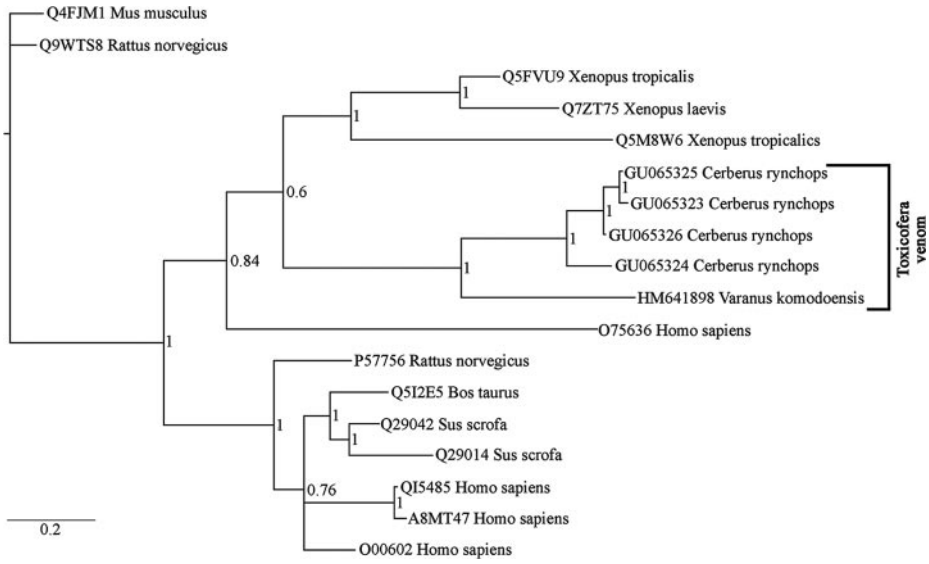

FIG. 8. **Bayesian phylogenetic reconstruction of veficolin toxins and related non-toxin ficolin sequences.**

TABLE II
Novel toxin types recovered from Anguimorpha lizard mandibular venom gland cDNA libraries

Toxin type	Species	GenBank accession no.	Bioactivity
Celestoxin	*C. warreni*	GU441474, GU441475	Shown in this study to be hypotensive (Fig. 11)
Cholecystoxin	*V. varius*	GU441461	Shown in this study to bind CCK-A receptor (Fig. 9)
Epididymal secretory protein	*V. gouldii*, *V. indicus*, *V. komodoensis*,	GU441519, GU441520, GU441521, GU441522, GU441523	Uncharacterized
Goannatyrotoxin	*V. eremius*	GU441529	Shown in this study to have a hypertensive/hypotensive triphasic effect (Fig. 10, *B* and *C*)
Ribonuclease	*G. infernalis*	GU441512, GU441513, GU441514, GU441515, GU441516, GU441517, GU441518,	Uncharacterized

prolonged hypotension), the frog skin YY peptides have broad spectrum antibiotic activity (32, 33). The hypotensive celestoxins did not display significant homology to any known peptide type. We also recovered from the libraries two protein types (epididymal secretory protein and ribonuclease) normally expressed in myriad non-salivary tissues and with a diversity of ancestral bioactivities (Table III).

The significant differences between the *H. suspectum cinctum* kallikrein toxins obtained in this study and the previously reported kallikrein toxin from *H. horridum* venom (P43685) (34) must be noted. This is particularly in stark contrast with the high degree of similarity of our *H. suspectum cinctum* toxins with other anguimorph lizard kallikrein toxins (Fig. 5). Our sequence alignments show that the tertiary structure determined by cysteine bonds is likely to be affected if the previously reported sequence P43685 is indeed correct. P43685 was reported as having 13 cysteines (missing the second ancestral cysteine with two new cysteines in atypical positions). Conspicuously, the last cysteine of the *H. horridum* sequence is absent from all other lizard toxin sequences previously reported or recovered in this study but is instead a characteristic of snake venom isoforms. Another significant difference between the helodermatid sequences is an insertion in P43685 at positions 126–132 that is not present in any of the clones from this study or any of the previously reported varanid lizard kallikrein toxins. These sequence differences are markedly higher than analogous sequence differences in CRiSP, exendin, lethal toxin 1, or PLA_2 between both *Heloderma* species. RT-PCR investigations revealed that primers designed using the reported *H. horridum* sequence P43685 did not react with *H. horridum* cDNA, whereas conversely, primers designed utilizing our *H. suspectum* sequence EU790962 from this study reacted strongly with the *H. horridum* cDNA library (Fig. 3*C*). Sequencing of the kallikrein isoform encoded in our *H. horridum* cDNA library (GenBank accession number HM437246) revealed it to be very similar to our *H. suspectum* sequence although contrasting starkly with the reported P43685 sequence. Thus, we conclude that the

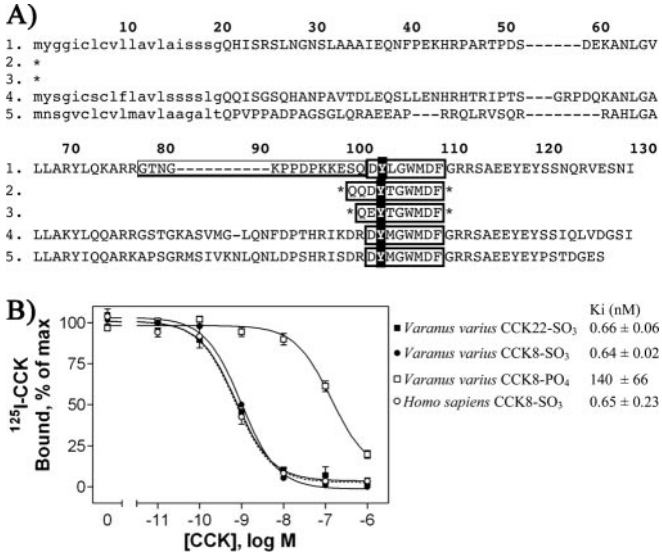

FIG. 9. *A*, sequence alignment of precursors of *V. varius* cholecystoxin (GU441461) (*1*) from the mandibular venom gland, the frog skin defensive skin toxins from *Litoria xanthomera* (P56264) (*2*) and *Phyllomedusa sauvagei* (Q7LZC4) (*3*), and the body peptides from *Python molurus* (Q8JHB9) (*4*) and *Homo sapiens* (P06307) (*5*). A *box* indicates a minimal bioactive processed peptide (both the long (22-amino acid) and short (eight-amino acid) forms of *V. varius* cholecystoxin (GU441461) are shown). *Y* with a *black background* represents the key bioactive post-translationally modified sulfatyrosine. * designates the only bioactive peptide domains sequenced to date. *B*, relative binding of cholecystokinin receptor A of the two variants highlighted in *boxes* in *A* (one is 22 amino acids, and one is eight amino acids), a variant of CCK8 with a phosphotyrosine instead of the sulfatyrosine, and human CCK8 with a sulfatyrosine.

previously reported *H. horridum* sequence P43685 (34)contains multiple errors. The impact of this is not limited to interpretations of lizard venom molecular evolution but also decimates the central conclusion of a study that examined convergent mutation in kallikrein toxins between helodermatid lizards and shrews and in particular relied upon the questionable insert at alignment position 126–132 as a key element (35).

Toxin Structure-Function Relationships—Our functional testing of cholecystoxin, celestoxin, goannatyrotoxin, helokinestatin, and natriuretic peptide analogs demonstrated that all these peptide toxins target the vascular smooth muscle. We were able to demonstrate that the cholecystoxin peptide activity is mediated by an eight-amino acid region with a post-translationally modified tyrosine (sulfated tyrosine) essential for activity, the same structure-function relationship as that of the mammalian endogenous body form (36, 37) (Fig. 9). Proline brackets also guided the activities of helokinestatin (Fig. 2*D*), goannatyrotoxin (Fig. 10), and celestoxin (Fig. 11) peptides.

Residue replacement studies of a novel natriuretic peptide from *G. infernalis* allowed us to demonstrate that both the aspartate at ring-position 7 and isoleucine at ring-position 9 contributed equally but both must be present for full activity in the endothelium-denuded aortic rings (Fig. 2*C*). The differential effect upon the mean arterial pressure of anesthetized animals, with the isoleucine 9 mutant producing a much greater effect than the aspartate 7 indicating action perhaps upon different pathways or receptor subtypes in the circulating systems. However, the variable bioactivity of other iso-

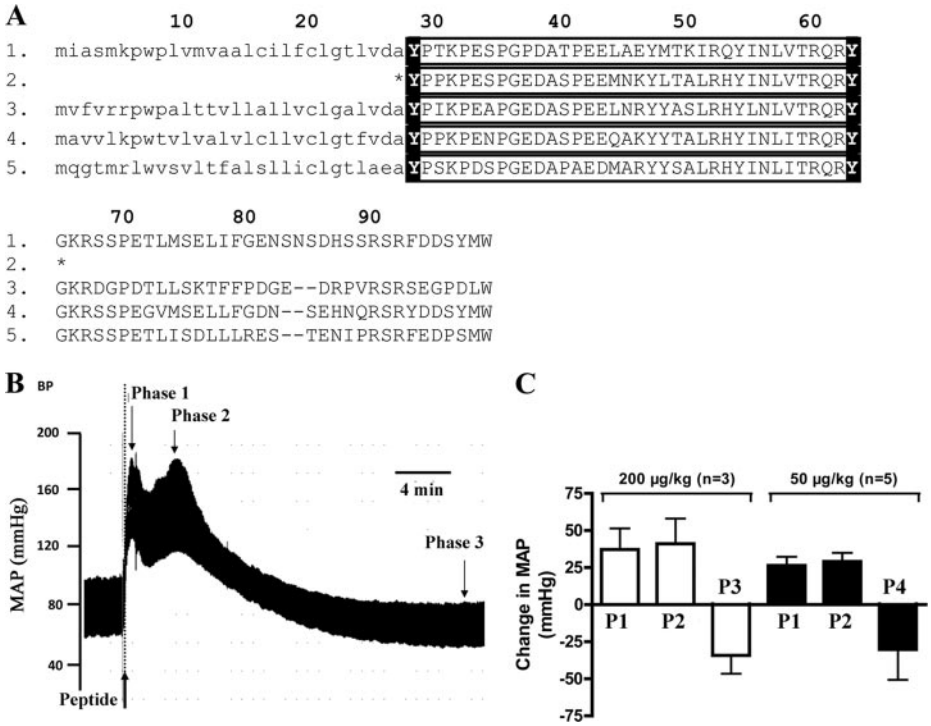

FIG. 10. *A*, sequence alignment of precursors of *V. eremius* goannatyrotoxin (GU441529) (*1*), the frog skin antimicrobial peptide P80952 from *Phyllomedusa bicolor* (*2*), and the related non-toxin, ordinary body peptides from *H. sapiens* (P10082) (*3*), *Anguilla japonica* (Q76CL2) (*4*), and *Gallus gallus* (P28673) (*5*). A *box* indicates a post-translationally processed bioactive peptide. The *second Y* with a *black background* is in amide form. * designates the N and C termini of a post-translationally processed peptide sequence. *B* and *C*, effect of intravenous injection of *V. eremius* goannatyrotoxin (GU441529). *P1*, phase 1; *P2*, phase 2; *P3*, phase 3; *MAP*, mean arterial pressure.

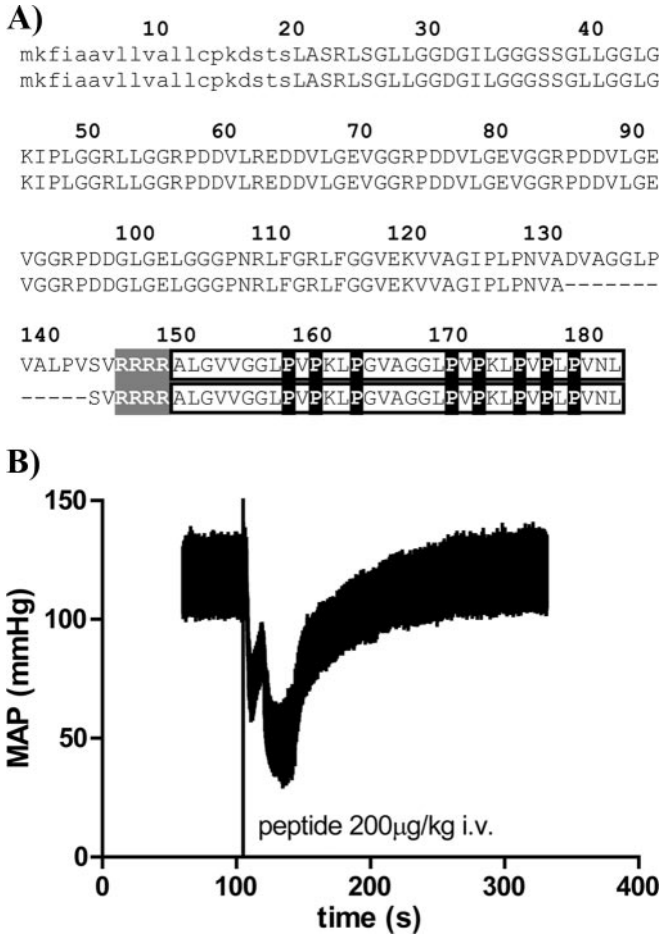

FIG. 11. *A*, sequence alignment of *C. warreni* celestoxin precursors from the mandibular venom gland (*1*, GU441474; *2*, GU441475). *Gray* highlights the cleavage motif. Bioactivity important prolines are highlighted in *black*. *B*, effect of intravenous (*i.v.*) injection of post-translationally cleaved peptide. The *vertical line* marks the time of injection. *MAP*, mean arterial pressure.

forms that contain these two invariant residues (GU441511 from *C. warreni* and GU441510 from *G. infernalis*) yet were only weakly active demonstrates that bioactivity is mediated by additional residues (Fig. 2*B*). The *C. warreni* isoform that is lessened in bioactivity contains the intraloop functional residues but does possess prolines in its C-tail (Fig. 2*B*). C-tail prolines have been shown previously to be responsible for the lessened activity of snake venom isoforms (16) and thus are the likely reason for the lowered activity of this isoform. In this isoform, either intraloop invariant residues are conserved or substitutions are present that did not affect the bioactivity of other characterized isoforms (*e.g.* His at loop position 4 that is also present in the potent *Dendroaspis* natriuretic peptide from *Dendroaspis angusticeps* (P28374)). However, a reduced bioactivity by the Arg-to-Lys change at ring position 8 cannot be ruled out as the two taipan inactive forms (16) have Arg-to-His changes at this position. The isoform GU441509 from *V. glauerti* is also poorly active (Fig. 2*B*) despite the conservation of this residue, and thus this change in GU441511 from *C. warreni* is not likely to be responsible for the loss of bioactivity; the proline-kinked tail is the more likely cause. Thus, the reduced activity in GU441509 from *V. glauerti* may be due to the otherwise invariant valine (non-polar) at ring position 12 being changed to threonine (polar).

Using our previously described methodology (18), molecular modeling studies revealed that several features are conserved in the CRiSPs investigated in this study (Fig. 4). Noteworthy are the conserved cysteine pattern and the tetrad in the PR1 domain, which was speculated to form part of an active site of unknown function (38). A third conserved feature is the structurally important residues, despite the extensive amount of cysteines, postulated by Guo *et al.* (38); albeit, we did not find all of the proposed amino acids conserved.

The suspected binding site in the CRiSP PR1 domain (38) is less conserved and is expected to affect substrate specificity if the proteins would indeed expose enzymatic activity. Of the three sequence patches lining up to form the postulated binding site, the first is the most conserved. After four highly variable positions, the following sequence motif could be deduced: [R](T/V)(I/V)*X*(G/K)(V/I/L)*X*[C][G][E][N]*X*(F/Y)*X*[S] (square brackets enclose conserved, functional residues). It has to be noted that where more than one residue occurs in a certain position the second and third amino acids are present in one case only. The second sequence stretch accounting for the putative substrate binding site (Fig. 4, alignment positions 130–138) could also be put into a sequence motif (although this motif is less conserved than the first motif), [G](P/A)*XX*(P/Q)*XX*(M/V/K)*X*, with variants such as alanine in position 2 in the snake toxin representatives *Trimeresurus stejnegeri* (P60623) and *Pseudechis australis* (Q8AVA4), glutamine in position 5 in the helodermatid sequences, and at position 8 valine in *T. stejnegeri* and *P. australis* and lysine in *V. tristis*. The third patch of amino acids to participate in substrate binding is variable (alignment 179–185).

Five residues in the CRiSP CRD were brought forward as possible interaction partners with K^+ channels (Fig. 4). In *T. stejnegeri*, these residues were Tyr^{150}, Cys^{212}, Thr^{213}, Arg^{214}, and Glu^{215} as well as the C-terminally located Phe^{244}. Whereas Tyr^{150} was supposed to only interact with the ion channel, the remaining residues were thought to be involved in the actual blocking of this protein. In *H. suspectum*, position 125 was a histidine rather than a tyrosine, the latter of which was observed in all other proteins studied. Not surprisingly, the cysteine in position 212 is conserved throughout all sequences because cysteines are predominantly involved in maintaining the three-dimensional structure of the proteins. The three residues following this cysteine are not conserved in CRiSPs. At each position, charged, polar, or non-polar amino acids were found in the proteins under investigation. Whereas in *T. stejnegeri* and *P. australis* two of these three amino acids are charged (Arg^{214} and Glu^{215} in *T. stejnegeri* and Lys^{213} and Arg^{215} in *P. australis*), only uncharged residues were found in

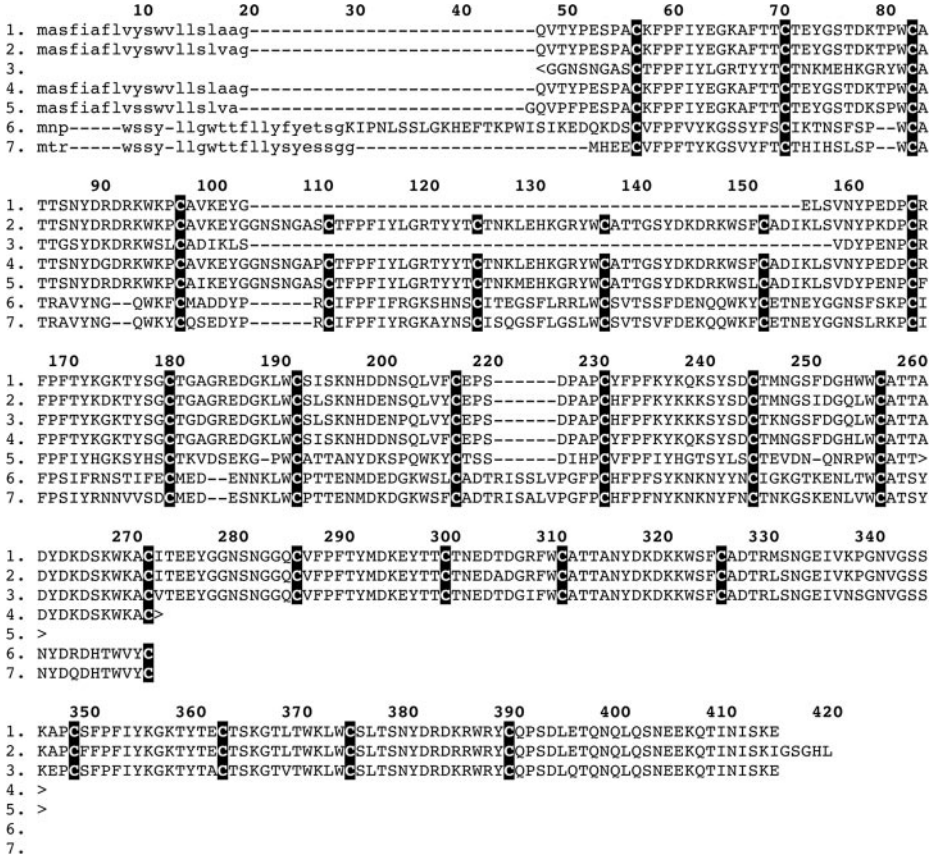

FIG. 12. **Sequence alignment of epididymal secretory protein precursors from mandibular venom glands (*1*–*5*) and related non-toxin body forms (*6* and *7*).** *1*, *V. komodoensis* (GU441521); *2*, *V. gouldii* (GU441519); *3*, *V. indicus* (GU441520); *4*, *V. komodoensis* (GU441522); *5*, *V. indicus* (GU441523); *6*, *Canis familiaris* (Q9GL25); *7*, *H. sapiens* (Q96BH3). < and > designate incomplete N and C termini of the precursor, respectively. ^ designates a protein sequencing fragment. Cysteines are in *black*.

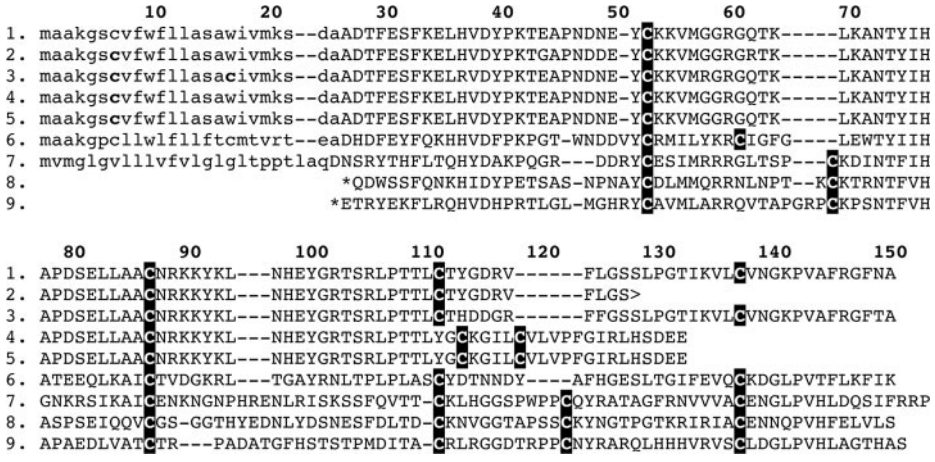

FIG. 13. **Sequence alignment of ribonuclease precursors.** Shown are *G. infernalis* (*1*, GU441512; *2*, GU441513; *3*, GU441514; *4*, GU441516; *5*, GU441517) and *C. warreni* (*6*, GU441518) mandibular venom glands and the related non-toxin body forms from *H. sapiens* (*7*, P03950), *Iguana iguana* (*8*, P80287), and *G. gallus* (*9*, P81476). > designates an incomplete C terminus of the precursor. * designates an N-terminal post-translationally processed protein sequence. Cysteines are in *black*.

V. varius and *G. infernalis*. The same applied for the residues in position Phe[244] in *T. stejnegeri*, although all residues in this position contain a quite bulky side chain. There are two possible interpretations for these findings. 1) The residues under investigation are not involved in the blocking of ion channels, *i.e.* K^+ channels. 2) Different CRiSPs interact with different ion channels, which contain different selectivity filters. The latter fact cannot be ruled out completely because it is known that *e.g.* the selectivity filters of ion channels may consist of both basic and acidic amino acids as well as uncharged amino acids (see Ref. 39). Thus, from the nature of amino acid modifications in this region as well, it can be inferred that, despite the high degree of overall sequence conservation between the CRiSP toxins of both helodermatid species as compared with CRiSPs from other anguimorph species, these toxins may interact with different ion channel isoforms.

Utilizing molecular modeling techniques as previously described by us (18), we also observed that the anguimorph CRiSPs contained three conserved surface histidines (His[82], His[140], and His[232]). All three histidines are at least partially exposed to solvent, which is of particular interest with regard

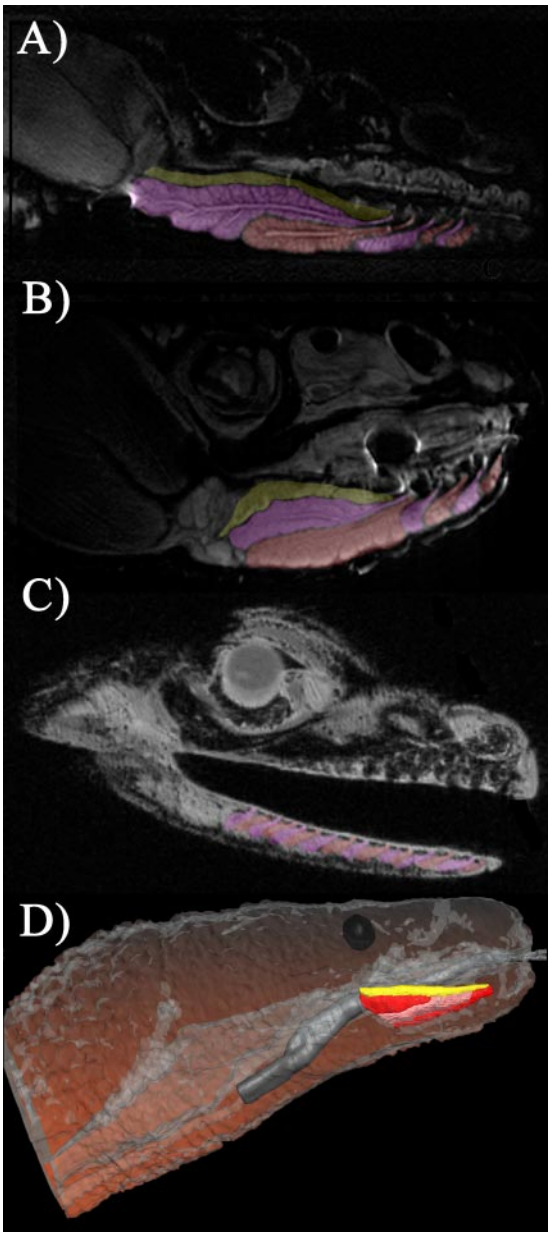

FIG. 14. Longitudinal MRI sectioning of *H. horridum* (*A*) and *H. suspectum* (*B*) shows the large ducts emerging separately from each compartment of the mandibular venom gland and terminating at the base of successive teeth. Mandibular venom gland compartments are arbitrarily alternately colored *red* and *purple*. In regard to MRI, note that curved multiplanar angulations of cross-sections were set differently for both animals to get optimal visualization of the lobes and ducts. This leads to a skewed impression of the shape of the anatomy (head and glands) relative to the *in vivo* observations such as in Ref. 1, and the differential slice angles also skew the relative presentation of gland gross morphology. *C*, longitudinal MRI section of *G. infernalis* with false coloring of mandibular venom gland compartments (arbitrarily alternately colored *red* and *purple*). *D*, three-dimensional reconstruction of *L. borneensis* mandibular venom gland compartments (arbitrarily falsely colored *red* and *purple*), showing the three-compartment arrangement consistent with previous histology and infralabial glands shown in *yellow* (2).

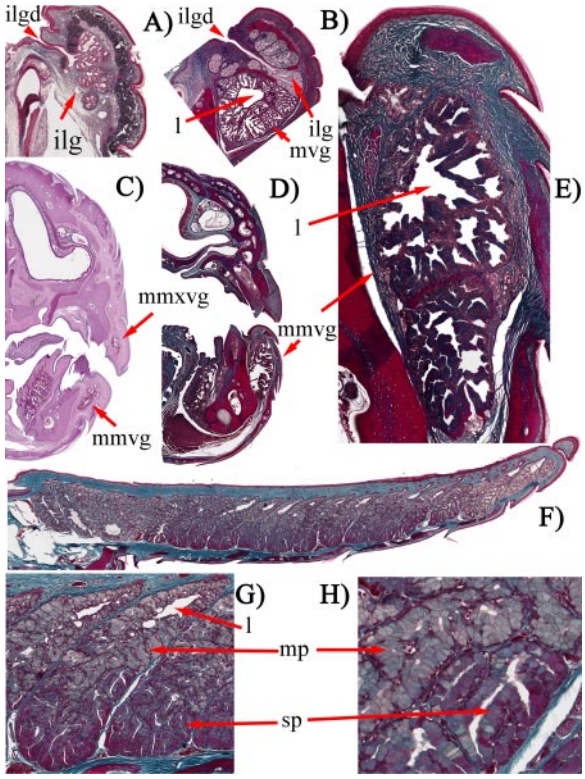

FIG. 15. *A*, Masson's trichrome-stained transverse histology section of *S. crocodilurus* showing the mixed seromucous lobules. *B*, Masson's trichrome-stained transverse histology section of *V. varius* showing the intratubular lumina feeding into the large central lumen of the mandibular venom gland and the individual mucous lobules dorsally positioned that collectively make up the gland. *C*, periodic acid-Schiff-stained transverse histology section of *O. apodus* revealing that small mandibular mixed type venom gland and small maxillary mixed type venom gland arrangements are present, each with a central lumen. Masson's trichrome-stained histology sections of the *G. infernalis* mixed mandibular venom gland show the intratubular lumina that feed into the large central lumen (*D*) and longitudinal (*E*) and transverse sections (*F*, *G*, and *H*). *ilg*, infralabial gland; *ilgd*, infralabial gland duct; *l*, lumen; *mmvg*, mixed mandibular venom gland; *mmxvg*, mixed maxillary venom gland; *mp*, mucous part; *mvg*, mandibular venom gland; *sp*, serous part.

to their side chain chemistry. This is of particular interest if one takes into account the pK_a value of the δ-NH in the imidazole ring of the histidine side chain. The side chain pK_a in free histidine is 6.02. However, this value may vary in protein environment. Because the venom pH is acidic (*e.g.* pH 5 for *Bothrops jararaca* (40)), it can be assumed that in venom most of these solvent-exposed histidines are protonated. When an anguimorph lizard (or snake for that matter) bites, venom is transferred into the blood stream of the prey, and the venom proteins are thus exposed to a physiological pH of 7.3. At this pH, the surface histidine side chains are mostly deprotonated, which could affect the functionality and possibly the toxicity of CRiSPs after administration.

In addition to changes in functional residues, neofunctionalisation may also be facilitated through changes in tertiary

TABLE III
Tissue locations for secretion and bioactivities of nearest related non-venom proteins for novel toxin types discovered in this study

Toxin	Tissue type for normal secretion	Bioactivity of ancestral protein
Celestoxin	No match	Unknown
Cholecystoxin (cholecystokinin)	Expressed in brain, lung, testis, and throughout the length of the small intestine; in the brain, expressed predominantly in the optic tectum and brain stem	Myriad including induction of gastric secretion, stimulation of pancreatic secretion, increase of blood circulation and water secretion in the stomach and intestine, and stimulation of smooth muscle contraction
Epididymal secretory protein	Epididymis	Unknown
Goannatyrotoxin (YY peptide)	Intestine	Inhibits exocrine pancreatic secretion, has a vasoconstrictory action, and inhibits jejunal and colonic mobility
Ribonuclease	Expressed predominantly in the pancreas	Pyrimidine-specific C-preferring nuclease

structure as a result of variations in the pattern and number of cysteines. Such changes were evident in CRiSP (Figure 4), kallikrein (Figure 5), epididymal secretory protein sequences (Figure 12), and ribonuclease (Figure 13). In both of the CRiSP variants with newly evolved cysteines (GU441473 from *C. warreni*, and GU441469 & GU441470 *V. indicus*), this results in an odd-number of cysteines, thus potentially resulting in dimerisation. Further, the *V. indicus* sequences have a truncation leading to the loss of six cysteines. In the novel anguiid kallikrein toxins GU441496 from *C. warreni* and GU441502 from *G. infernalis* have deletions ancestral cysteines combined with the evolution of new cysteines. The variants recovered from *V. acanthurus* (Q2XXN1) and *V. scalaris* (GU441486) may also form a dimer as a result of a newly evoled cysteine resulting in an odd-number of cysteines. The venom epididymal secretory protein sequnces recovered from the *Varanus* libraries have additional eight cysteines present. In addition, an addtional mutation deleted four of the twenty cysteines. Such variation was present in two species (*V. indicus* and *V. komodoensis*), both of which also possessed an isoform that did not have this deletion, indicating that this mutation occured prior to speciation from their common ancestor in one of the isoforms present at that time. The basal type ribonuclease toxin sequences (recovered from both *C. warreni* and *G. infernalis*) have deletions of two ancestral cysteines. The two isoforms of a derived variant recovered from the *G. infernalis* library have a frame-shift mutation near the C-terminal, resulting not only in slight truncated sequnces and the loss of two of the ancestral cysteines, but also producing two new cysteines.

Timing of Toxin Recruitment Events and of Functional Diversification—Particularly notable was our identification of two additional toxin types (lectin and hyaluronidase) that share an ancient homology with toxins from snake venoms and thus form part of the core Toxicofera arsenal (Fig. 1). We were also able to determine the timing of diversification of the crucial tripeptide lectin toxin functional motif. Previously, based upon snake toxin studies, it was hypothesized that the EPN variation, which mediates antiplatelet activity through the utilization of the mannose binding site (41), was basal to all snake venoms, whereas the QPD variant, which utilizes the galactose binding site (41), was more recently derived within snake venoms (18). However, both motifs were recovered in this study (*O. apodus* and *V. indicus*, respectively) (Fig. 16). Therefore, as both motifs are basal to all toxicoferan venoms, it is unclear which is the ancestral state and which was an early derivation. Although hyaluronidase activity has been reported previously for *Heloderma* venom (42), lack of sequence data prevented determination of molecular identity and thus the relative relationship to the snake toxin forms, which themselves have only been recently sequenced (18, 43). Our sequencing of lizard venom hyaluronidase from both *H. suspectum* and *G. infernalis* allowed for the determination that not only was this a basal lizard venom toxin type but that it was indeed a toxin basal to all Toxicofera venoms (Fig. 1).

It had been previously unclear whether the exendin peptides were founded by a recruitment of a glucagon-like or VIP-like peptide (22). The relative presence of exendin peptides in *Heloderma* venoms was investigated through primer-directed sequencing with the aim to determine the relative timing of diversification between the ancestral glucagon-derived exendin-3 and -4, which are less toxic (22), and the more recently derived exendin-1 and -2, which contain the more potent VIP-like domain. It was shown that exendin-1 is present in only very low levels in *H. horridum*, whereas exendin-2 is absent entirely. Our results confirm a glucagon peptide ancestry of the exendin peptides. The molecular evolution of the VIP domain precedes the *H. horridum*/*suspectum* speciation event, but the duplication of exendin-1 to additionally produce exendin-2 postdates speciation (Fig. 1). The high levels of exendin-1 in *H. suspectum* but not *H. horridum* may be linked to the significant ecological niche occupation and size difference between the two species.

For the natriuretic peptides, we were able to elucidate the timing of domain mutations that additionally encode for the post-translationally liberated proline-rich helokinestatin peptides; the helokinestatins are a derivation that occurred basally to the anguid/helodermatid clade (Figs. 1, 2, and 7). We were also able to resolve the relationship to snake venom forms; lizard and snake toxin forms are in distinct clades separated by ordinary body forms and thus represent independent toxin recruitment events (Fig. 7). However, as with

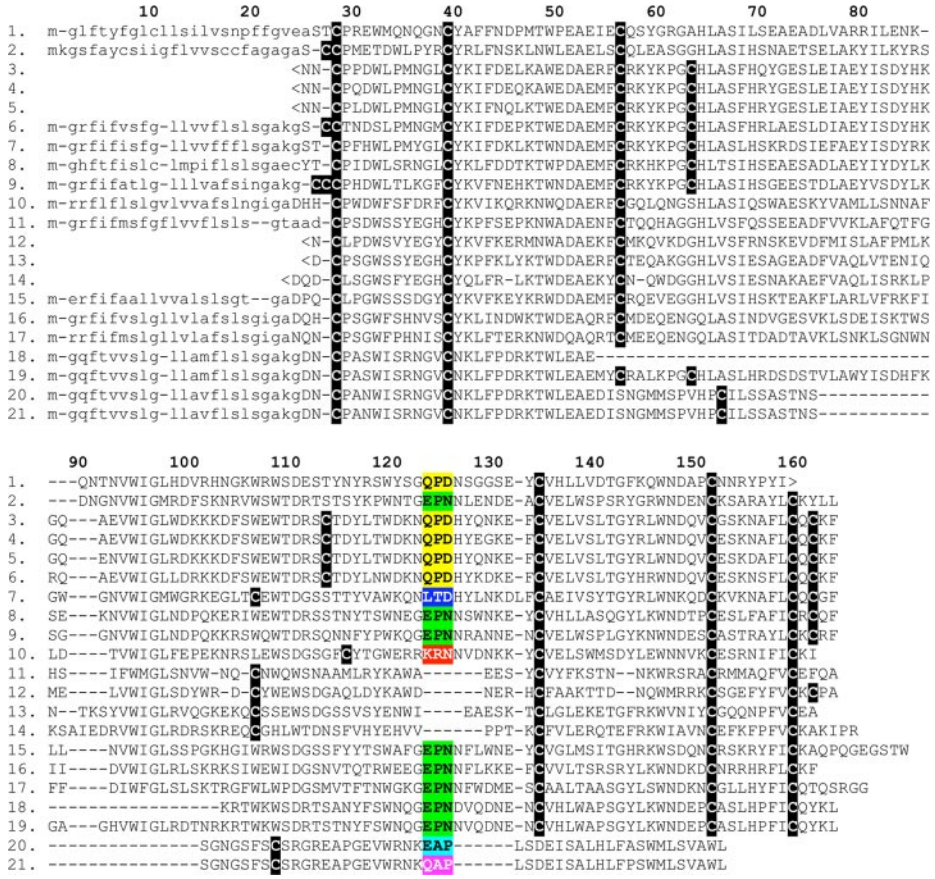

FIG. 16. **Sequence alignment of lectin toxin precursors.** *1*, *O. apodus* (GU441505); *2*, *V. indicus* (GU441506); *3*, *Bitis gabonica* (Q9PSN0); *4*, *Lachesis stenophrys* (Q9PSM4); *5*, *Crotalus atrox* (P21963); *6*, *T. stejnegeri* (Q9YGP1); *7*, *B. gabonica* (Q6T7B7); *8*, *Micrurus corallinus* (56); *9*, *Thrasops jacksoni* (EU029696); *10*, *Leiheterodon madagascariensis* (EU029699); *11*, *Protobothrops flavoviridis* β-chain (P23807); *12*, *Echis carinatus* β-chain (P81996); *13*, *P. flavoviridis* α-chain (Q7LZ71); *14*, *E. carinatus* α-chain (P81017); *15*, *Liophis poecilogyrus* (EU029697); *16*, *Philodryas olfersii* (EU029700); *17*, *L. poecilogyrus* (EU029702), and *18–21*, *Enhydris polylepis* (*18*, EU029689; *19*, EU029691; *20*, EU091713; *21*, EU091711). < and > designate incomplete N and C termini of the precursor, respectively. Cysteines are in *black*. Variants of the functional tripeptide are *colored*.

the convergent recruitment of PLA_2 genes for use as toxins in snake and lizard venoms (13, 19, 44), different types of natriuretic body peptides were recruited for toxic mutation. The lizard toxins are within the BNP clade, whereas the snake toxins are within the CNP clade.

Phylogenetic structure exists within the snake toxins both in the presence of derived proline-rich molecules and in the presence of a derived C-terminal tail. Within the tail-less snake venom isoforms, the gene has also been convergently mutated to encode for additional, post-translationally cleaved proline-rich peptides within the viperid snakes: pit viper natriuretic genes additionally encode for bradykinin-potentiating peptides (see Ref. 45), whereas the *Echis* genus of true vipers encodes metalloprotease-inhibiting peptides (46). Although the snake venom natriuretic peptides are founded by a tail-less CNP gene, some forms possess a derived C-terminal tail and form a subclade within the main tail-less clade and thus represent a recent derivation (Fig. 7). While the tail-less snake natriuretic toxins bind the guanylyl cyclase B receptor, the derived forms with C-terminal tails instead bind the guanylyl cyclase A receptor (16). Thus the derived C-terminal tail possessing snake natriuretic toxins are convergent bothin tail and targeting with the C-terminal tail possessing, guanylyl cyclase A binding lizard natriuretic toxins.

Derivations of Venom System—We have shown previously that in snake species that have developed secondary forms of prey capture (*e.g.* constricting) or switched to feeding on eggs the reptile venom system undergoes rapid degeneration characterized by significant atrophying of the glands, reduction in fang length, and accumulated deleterious mutations in the genes encoding for the venom proteins (18, 47, 48). This is a consequence of selection pressure against the bioenergetic cost of protein production (49). In the lizard *V. komodoensis*, the robust glands and high venom yield thus argued for active use of the venom system (20). Therefore, as the Anguimorpha glands are not only retained but continue to diversify, this argues for active evolution operating under selection pressure.

Previous anatomical studies of *Heloderma* mandibular venom glands used traditional dissection and histological methods and reported a single ducted gland for *H. horridum* and variably three to five compartments for the *H. suspectum* venom gland (1, 3, 50–53). By using MRI, here we found that there instead are six compartments in both with each compartment with its own duct that terminates at the base of the grooved teeth (Fig. 14, *A* and *B*). In contrast, although the varanid lizards also have independently derived six compartments, the compartment structures are distinct from those of the helodermatids (compare Fig. 14, *A* and *B*, with Ref. 20),

and the varanid compartment ducts terminate between successive bladelike teeth as noted previously for *V. komodoensis* (20).

The architecture of the mandibular venom glands of the Anguimorpha shows two modes (Figs. 14 and 15): a mixed sero/mucous arrangement (anguids) or an encapsulated protein gland (helodermatids and varanids). In the Anguidae, the gland has one compartment per tooth. Extensive intralumen drainage channeling was evident, but the major lumen is unstructured. In contrast are the independently derived encapsulated forms in *Heloderma* and in the *Lanthanotus*/*Varanus* clade. Segregation of the protein- and mucus-secreting regions and encapsulation of the protein glands occurred independently twice with the *Heloderma* and the *Lanthanotus*/*Varanus* arrangements representing independent derivations of the system (Figs. 1, 14, and 15). In both cases, posterior compartments were fused, thus increasing lumen storage space. Extensive intralumen drainage channeling in both cases feeds into highly structured lumens.

Although the adaptive significance and evolutionary polarity of the Anguimorph lizard venom gland variation are unclear, the glands are evidently more complex than reported previously (Fig. 14) and emphasize the notion that substantial evolutionary innovation of any aspect of the venom system can occur even among closely related species in this genus. To understand the evolutionary pressures responsible for the variation in gland structure, we need more information on the ecology, particularly feeding, on the one hand and on the function of the secretion epithelium and venom delivery on the other. Examination of variation in venom gland architecture and development across the group and beyond might provide further insights into the structure variability (increase or decrease in compartmentalization) and, together with differences in venom composition, explain the ecological and evolutionary significance of the entire venom apparatus. The retention of the ancestral maxillary and mandibular gland arrangement in *O. apodus* (Fig. 15) is particularly intriguing.

Conclusion—Our major findings are of a multidisciplinary nature with uses ranging from evolutionary biology to protein evolution and highlight the underutilization of lizard venom as bioresources in drug design and development. Collectively, these findings strongly support the notion that during the long evolutionary history of the 130 million-year-old Anguimorpha lizard radiation (54) there has been extensive modification of the venom system. All variables appear to change independently, ranging from the biochemical variation and specialization of the venoms to the glandular morphology. We still know little about the venom macroevolution and the potential role in the ecology/evolution of the animals themselves. We do not know enough of composition, the role of individual venom components in prey capture, or *in vitro* activities. Furthermore, the toxin types recovered in this study should not be considered as the full suite because the relatively limited sampling only recovered the dominant forms. More extensive sampling will no doubt recover novel isoforms of types identified to date as well as entirely new toxin classes. In addition, the relationships of transcriptomes to proteomes may reveal translational variances as has been documented for snakes (see Ref. 55).

However, we may safely assume that in common with snake venoms these lizard venoms possess a high potential for drug lead discovery as evidenced by the commercial success of an exendin-4 toxin analog (from *Heloderma* venom) in reaching the marketplace as the drug Byetta™ to treat type 2 diabetes. Underscoring their biodiscovery potential was our finding of three novel peptide types with potent and unique activities upon the cardiovascular system. Our structure-function studies provide data supporting the notion that anguimorph lizard venoms, although posing trivial human medical implications (with the exception of helodermatid species or large varanids such as *V. komodoensis*), provide interesting and unexploited templates for pharmacoecological studies. We would also like to emphasize that these species belong to an ever growing group of threatened species that may affect biodiversity and cause an important loss of genetic information. We therefore hope that this study will not only stimulate further research and provide a new understanding and realization of conservation efforts but will also encourage the utilization of this precious natural resource in a sustainable and ethical manner.

Acknowledgments—We express our deep gratitude to the Naturalis Museum for allowing access to a *L. borneensis* specimen for MRI scanning. The California Academy of Sciences generously loaned us preserved specimens for magnetic resonance imaging studies; we are deeply grateful to Jens Vindum for facilitating this scientific exchange. We also thank Chip Cochran and Cale Morris for help in specimen collection.

* This work was supported by grants from the Australian Research Council (to B. G. F. and J. A. N.), a Fonds Wetenschappelijk Onderzoek-Vlaanderen postdoctoral fellowship (to K. R.), and funding from the Ian Potter Foundation (to F. L.).

The nucleotide sequence(s) reported in this paper has been submitted to the GenBank™EBI Data Bank with accession number(s) EU790958, EU790961, EU790962, EU790965–EU790968, GU441461–GU441529, and HM437246.

[b] To whom correspondence should be addressed. E-mail: bgf@unimelb.edu.au.

REFERENCES

1. Kochva, E. (1974) Specialized glands of the lower jaw in anguimorphs, in *Recherches Biologiques Contemporaines, Dedicated to the Memory of Dr. Manfred Gabe (1916–1973),* L. Arvy (Ed.), Imprimerie Vagner, Nancy, France, 281–286
2. Kochva, E. (1978) Oral glands of the Reptilia, in *Biology of the Reptilia* (Gans, C., and Gans, K. A., eds) pp. 43–161, Academic Press, London
3. Saint Girons, H. (1988) The cephalic exocrine glands of the reptiles. I. Anatomical and histological data. *Ann. Sci. Nat. Zool.* **9,** 221–255
4. Fry, B. G., Vidal, N., Norman, J. A., Vonk, F. J., Scheib, H., Ramjan, S. F., Kuruppu, S., Fung, K., Hedges, S. B., Richardson, M. K., Hodgson, W. C., Ignjatovic, V., Summerhayes, R., and Kochva, E. (2006) Early evolution of the venom system in lizards and snakes. *Nature* **439,**

584–588
5. Vidal, N., and Hedges, S. B. (2005) The phylogeny of squamate reptiles (lizards, snakes, and amphisbaenians) inferred from nine nuclear protein-coding genes. *C. R. Biol.* **328,** 1000–1008
6. Arano-Sánchez, D. (2008) Envenomation by a wild Guatemalan beaded lizard *Heloderma horridum charlesbogerti. Clin. Toxicol.* **46,** 897–899
7. Beck, D. D. (2005) *Biology of Gila Monsters and Beaded Lizards*, University of California Press, Berkeley, CA
8. Bogert, C. M., and del Campo, R. M. (1956) The Gila monster and its allies. The relationships, habits, and behavior of the lizards of the family Helodermatidae. *Bull. Am. Mus. Nat. Hist.* **109**, 1–238
9. Bou-Abboud, C. F., and Kardassakis, D. G. (1988) Acute myocardial-infarction following a Gila monster (*Heloderma suspectum cinctum*) bite. *West. J. Med.* **148,** 577–579
10. Cantrell, F. L. (2003) Envenomation by the Mexican beaded lizard: a case report. *J. Toxicol. Clin. Toxicol.* **41,** 241–244
11. Hooker, K. R., Caravati, E. M., and Hartsell, S. C. (1994) Gila monster envenomation. *Ann. Emerg. Med.* **24,** 731–735
12. Strimple, P. D., Tomassoni, A. J., Otten, E. J., and Bahner, D. (1997) Report on envenomation by a Gila monster (*Heloderma suspectum*) with a discussion of venom apparatus, clinical findings, and treatment. *Wilderness Environ. Med.* **8,** 111–116
13. Fry, B. G. (2005) From genome to "venome": molecular origin and evolution of the snake venom proteome inferred from phylogenetic analysis of toxin sequences and related body proteins. *Genome Res.* **15,** 403–420
14. Fry, B. G., Wüster, W., Kini, R. M., Brusic, V., Khan, A., Venkataraman, D., and Rooney, A. P. (2003) Molecular evolution and phylogeny of elapid snake venom three-finger toxins. *J. Mol. Evol.* **57,** 110–129
15. Rodríguezde la Vega, R. C., Merino, E., Becerril, B., and Possani, L. D. (2003) Novel interactions between K+ channels and scorpion toxins. *Trends Pharmacol. Sci.* **24,** 222–227
16. Fry, B. G., Wickramaratana, J. C., Lemme, S., Beuve, A., Garbers, D., Hodgson, W. C., and Alewood, P. (2005) Novel natriuretic peptides from the venom of the inland taipan (*Oxyuranus microlepidotus*): isolation, chemical and biological characterisation. *Biochem. Biophys. Res. Commun.* **327,** 1011–1015
17. Mouhat, S., Jouirou, B., Mosbah, A., De Waard, M., and Sabatier, J. M. (2004) Diversity of folds in animal toxins acting on ion channels. *Biochem. J.* **378,** 717–726
18. Fry, B. G., Scheib, H., van der Weerd, L., Young, B., McNaughtan, J., Ramjan, S. F., Vidal, N., Poelmann, R. E., and Norman, J. A. (2008) Evolution of an arsenal. *Mol. Cell. Proteomics* **7,** 215–246
19. Fry, B. G., Vidal, N., van der Weerd, L., Kochva, E., and Renjifo, C. (2009) Evolution and diversification of the Toxicofera reptile venom system. *J. Proteomics* **72,** 127–136
20. Fry, B. G., Wroe, S., Teeuwisse, W., van Osch, M. J., Moreno, K., Ingle, J., McHenry, C., Ferrara, T., Clausen, P., Scheib, H., Winter, K. L., Greisman, L., Roelants, K., van der Weerd, L., Clemente, C. J., Giannakis, E., Hodgson, W. C., Luz, S., Martelli, P., Krishnasamy, K., Kochva, E., Kwok, H. F., Scanlon, D., Karas, J., Citron, D. M., Goldstein, E. J., McNaughtan, J. E., and Norman, J. A. (2009) A central role for venom in predation by *Varanus komodoensis* (Komodo Dragon) and the extinct giant Varanus (Megalania) priscus. *Proc. Natl. Acad. Sci. U.S.A.* **106,** 8969–8974
21. Thompson, G. G., Clemente, C. J., Withers, P. C., Fry, B. G., and Norman, J. A. (2008) Is body shape of varanid lizards linked with retreat choice? *Aust. J. Zool.* **56,** 351–362
22. Fry, B. G., Roelants, K., Winter, K., Hodgson, W. C., Griesman, L., Kwok, H. F., Scanlon, D., Karas, J., Shaw, C., Wong, L., and Norman, J. A. (2010) Novel venom proteins produced by differential domain-expression strategies in Beaded Lizards and Gila Monsters (genus *Heloderma*). *Mol. Biol. Evol.* **27,** 395–407
23. Fry, B. G., Roelants, K., Champagne, D. E., Scheib, H., Tyndall, J. D., King, G. F., Nevalainen, T. J., Norman, J. A., Lewis, R. J., Norton, R. S., Renjifo, C., and de la Vega, R. C. (2009) The toxicogenomic multiverse: convergent recruitment of proteins into animal venoms. *Annu. Rev. Genomics Hum. Genet.* **10,** 483–511
24. Kwok, H. F., Chen, T., O'Rourke, M., Ivanyi, C., Hirst, D., and Shaw, C. (2008) Helokinestatin: a new bradykinin B-2 receptor antagonist decapeptide from lizard venom. *Peptides* **29,** 65–72
25. Junqueira-de-Azevedo Ide, L., and Ho, P. L. (2002) A survey of gene expression and diversity in the venom glands of the pitviper snake Bothrops insularis through the generation of expressed sequence tags (ESTs). *Gene* **299,** 279–291
26. Wagstaff, S. C., and Harrison, R. A. (2006) Venom gland EST analysis of the saw-scaled viper, *Echis ocellatus*, reveals novel alpha(9)beta(1) integrin-binding motifs in venom metalloproteinases and a new group of putative toxins, renin-like aspartic proteases. *Gene* **377,** 21–32
27. Hook, V., Funkelstein, L., Lu, D., Bark, S., Wegrzyn, J., and Hwang, S. R. (2008) Proteases for processing proneuropeptides into peptide neurotransmitters and hormones. *Annu. Rev. Pharmacol. Toxicol.* **48,** 393–423
28. Veenstra, J. A. (2000) Mono- and dibasic proteolytic cleavage sites in insect neuroendocrine peptide precursors. *Arch. Insect Biochem. Physiol.* **43,** 49–63
29. Trajanovska, S., and Donald, J. A. (2008) Molecular cloning of natriuretic peptides from the heart of reptiles: loss of ANP in diapsid reptiles and birds. *Gen. Comp. Endocrinol.* **156,** 339–346
30. Ching, A. T., Rocha, M. M., Paes Leme, A. F., Pimenta, D. C., de Fátima, D., Furtado, M., Serrano, S. M., Ho, P. L., and Junqueira-de-Azevedo, I. L. (2006) Some aspects of the venom proteome of the Colubridae snake *Philodryas olfersii* revealed from a Duvernoy's (venom) gland transcriptome. *FEBS Lett.* **580,** 4417–4422
31. Bowie, J. H., and Tyler, M. J. (2006) *Host Defense Peptides from Australian Amphibians: Caerulein and Other Neuropeptides*, Academic Press, San Diego, CA
32. Mor, A., Chartrel, N., Vaudry, H., and Nicolas, P. (1994) Skin peptide tyrosine-tyrosine, a member of the pancreatic-polypeptide family—isolation, structure, synthesis, and endocrine activity. *Proc. Natl. Acad. Sci. U.S.A.* **91,** 10295–10299
33. Vouldoukis, I., Shai, Y., Nicolas, P., and Mor, A. (1996) Broad spectrum antibiotic activity of skin-PYY. *FEBS Lett.* **380,** 237–240
34. Utaisincharoen, P., Mackessy, S. P., Miller, R. A., and Tu, A. T. (1993) Complete primary structure and biochemical-properties of gilatoxin, a serine-protease with kallikrein-like and angiotensin-degrading activities. *J. Biol. Chem.* **268,** 21975–21983
35. Aminetzach, Y. T., Srouji, J. R., Kong, C. Y., and Hoekstra, H. E. (2009) Convergent evolution of novel protein function in shrew and lizard venom. *Curr. Biol.* **19,** 1925–1931
36. Miller, L. J., and Lybrand, T. P. (2002) Molecular basis of agonist binding to the type A cholecystokinin receptor. *Pharmacol. Toxicol.* **91,** 282–285
37. Ondetti, M. A., Rubin, B., Engel, S. L., Pluscec, J., and Sheehan, J. T. (1970) Cholecystokinin-pancreozymin—recent developments. *Am. J. Dig. Dis.* **15,** 149–156
38. Guo, M., Teng, M., Niu, L., Liu, Q., Huang, Q., and Hao, Q. (2005) Crystal structure of the cysteine-rich secretory protein stecrisp reveals that the cysteine-rich domain has a K+ channel inhibitor-like fold. *J. Biol. Chem.* **280,** 12405–12412
39. Scheib, H., McLay, I., Guex, N., Clare, J. J., Blaney, F. E., Dale, T. J., Tate, S. N., and Robertson, G. M. (2006) Modeling the pore structure of voltage-gated sodium channels in closed, open, and fast-inactivated conformation reveals details of site 1 toxin and local anesthetic binding. *J. Mol. Model.* **12,** 813–822
40. Sousa, J. R., Monteiro, R. Q., Castro, H. C., and Zingali, R. B. (2001) Proteolytic action of Bothrops jararaca venom upon its own constituents. *Toxicon* **39,** 787–792
41. Drickamer, K. (1992) Engineering galactose-binding activity into a c-type mannose-binding protein. *Nature* **360,** 183–186
42. Tu, A. T., and Hendon, R. R. (1983) Characterization of lizard venom hyaluronidase and evidence for its action as a spreading factor. *Comp. Biochem. Physiol. B* **76,** 377–383
43. Harrison, R. A., Ibison, F., Wilbraham, D., and Wagstaff, S. C. (2007) Identification of cDNAs encoding viper venom hyaluronidases: cross-generic sequence conservation of full-length and unusually short variant transcripts. *Gene* **392,** 22–33
44. Fry, B. G., and Wüster, W. (2004) Assembling an arsenal: Origin and evolution of the snake venom proteome inferred from phylogenetic analysis of toxin sequences. *Mol. Biol. Evol.* **21,** 870–883
45. Soares, M. R., Oliveira-Carvalho, A. L., Wermelinger, L. S., Zingali, R. B., Ho, P. L., Junqueira-de-Azevedo, I. L., and Diniz, M. R. (2005) Identification of novel bradykinin-potentiating peptides and C-type natriuretic peptide from *Lachesis muta* venom. *Toxicon* **46,** 31–38
46. Wagstaff, S. C., Favreau, P., Cheneval, O., Laing, G. D., Wilkinson, M. C., Miller, R. L., Stöcklin, R., and Harrison, R. A. (2008) Molecular charac-

terisation of endogenous snake venom metalloproteinase inhibitors. *Biochem. Biophys. Res. Commun.* **365,** 650–656
47. Li, M., Fry, B. G., and Kini, R. M. (2005) Putting the brakes on snake venom evolution: the unique molecular evolutionary patterns of *Aipysuras eydouxii* (Marbled sea snake) phospholipase A(2) toxins. *Mol. Biol. Evol.* **22,** 934–941
48. Li, M., Fry, B. G., and Kini, R. M. (2005) Eggs-only diet: Its implications for the toxin profile changes and ecology of the marbled sea snake (*Aipysurus eydouxii*). *J. Mol. Evol.* **60,** 81–89
49. Akashi, H., and Gojobori, T. (2002) Metabolic efficiency and amino acid composition in the proteomes of *Escherichia coli* and *Bacillus subtilis. Proc. Natl. Acad. Sci. U.S.A.* **99,** 3695–3700
50. Gabe, M. and Saint Girons, H. (1969) Histological data on the salivary glands of the lepidosaurs. *Mem. Mus. Natl. Hist. Nat.* **58,** 1–118
51. Kochva, E. (1978) Evolution and secretion of venom and its antidotes in snakes. *Period. Biol.* **80,** 11–23
52. Saint Girons, H. (1989) The cephalic exocrine glands of the reptiles. II. Functional and evolutionary considerations. *Ann. Sci. Nat. Zool.* **104,** 1–17
53. Stewart, C. (1891) On some points in the anatomy of *Heloderma. Proc. Zool. Soc. Lond.* **59,** 119–121
54. Vidal, N., and Hedges, S. B. (2009) The molecular evolutionary tree of lizards, snakes, and amphisbaenians. *C. R. Biol.* **332,** 129–139
55. Sanz, L., Escolano, J., Ferretti, M., Biscoglio, M. J., Rivera, E., Crescenti, E. J., Angulo, Y., Lomonte, B., Gutiérrez, J. M., and Calvete, J. J. (2008) Snake venomics of the South and Central American Bushmasters. Comparison of the toxin composition of *Lachesis muta* gathered from proteomic versus transcriptomic analysis. *J. Proteomics* **71,** 46–60
56. Ho, P. L., Soares, M. B., Yamane, T., and Raw, I. (1995) Reverse biology applied to *Micrurus corallinus*, a South American coral snake. *J. Toxicol. Toxin Rev.* **14,** 327–337
57. Mochca-Morales, J., Martin, B. M., and Possani, L. D. (1990) Isolation and characterization of helothermine, a novel toxin from *Heloderma horridum horridum* (Mexican beaded lizard) venom. *Toxicon* **28,** 299–309
58. Morrissette, J., Elhayek, R., Possani, L., and Coronado, R. (1994) Isolation and characterization of ryanodine receptor toxins from *Heloderma horridum* (Mexican beaded lizard) venom. *Biophys. J.* **66,** A415–A415
59. Morrissette, J., Krätzschmar, J., Haendler, B., el-Hayek, R., Mochca-Morales, J., Martin, B. M., Patel, J. R., Moss, R. L., Schleuning, W. D., and Coronado, R. (1995) Primary structure and properties of helothermine, a peptide toxin that blocks ryanodine receptors. *Biophys. J.* **68,** 2280–2288
60. Nobile, M., Magnelli, V., Lagostena, L., Mochca-Morales, J., Possani, L. D., and Prestipino, G. (1994) The toxin helothermine affects potassium currents in newborn rat cerebellar granule cells. *J. Membr. Biol.* **139,** 49–55
61. Nobile, M., Noceti, F., Prestipino, G., and Possani, L. D. (1996) Helothermine, a lizard venom toxin, inhibits calcium current in cerebellar granules. *Exp. Brain Res.* **110,** 15–20
62. Mebs, D. (1969) Purification and properties of a kinin liberating enzyme from venom of *Heloderma suspectum. Naunyn-Schmiedebergs Arch. Pharmakol.* **264**, 280–281
63. Mebs, D. (1969) Isolation and properties of kallikrein from venom of Gila Monster (*Heloderma suspectum*). *Hoppe-Seyler's Z. Physiol. Chem.* **350**, 821–826
64. Nikai, T., Imai, K., Komori, Y., and Sugihara, H. (1992) Isolation and characterization of arginine ester hydrolase from *Heloderma horridum* (beaded lizard) venom. *Int. J. Biochem.* **24,** 415–420
65. Nikai, T., Imai, K., Sugihara, H., and Tu, A. T. (1988) Isolation and characterization of horridum toxin with arginine ester hydrolase activity from *Heloderma horridum* (Beaded lizard) venom. *Arch. Biochem. Biophys.* **264,** 270–280
66. Datta, G., and Tu, A. T. (1997) Structure and other chemical characterizations of gila toxin, a lethal toxin from lizard venom. *J. Pept. Res.* **50,** 443–450
67. Clemetson, K. J., Lu, Q., and Clemetson, J. M. (2005) Snake C-type lectin-like proteins and platelet receptors. *Pathophysiol. Haemost. Thromb.* **34,** 150–155
68. Morita, T. (2005) Structures and functions of snake venom CLPs (C-type lectin-like proteins) with anticoagulant-, procoagulant-, and platelet-modulating activities. *Toxicon* **45,** 1099–1114
69. Huang, T. F., and Chiang, H. S. (1994) Effect on human platelet-aggregation of phospholipase A(2) purified from *Heloderma horridum* (beaded lizard) venom. *Biochim. Biophys. Acta* **1211,** 61–68
70. Hadac, E. M., Ghanekar, D. V., Holicky, E. L., Pinon, D. I., Dougherty, R. W., Miller, L. J. (1996) Relationship between native and recombinant cholecystokinin receptors: Role of differential glycosylation Pancreas **13,** 130–139